TURUN YLIOPISTON JULKAISUJA
ANNALES UNIVERSITATIS TURKUENSIS

SARJA - SER. A I OSA - TOM. 448

ASTRONOMICA - CHEMICA - PHYSICA - MATHEMATICA

POROUS SILICON OPTICAL FILTERS IN GAS SENSING APPLICATIONS

by

Tero Jalkanen

TURUN YLIOPISTO
UNIVERSITY OF TURKU
Turku 2012

From

Department of Physics and Astronomy
University of Turku
FI-20014 Turku
Finland

Supervised by

Jarno Salonen
Docent
Department of Physics and Astronomy
University of Turku
Finland

Reviewed by

Sharon M. Weiss
Associate Professor
Department of Electrical Engineering & Computer Science
Vanderbilt University
United States of America

Luca De Stefano
Senior Researcher
Institute for Microelectronics and Microsystems
National Research Council
Italy

Opponent

Nicolas H. Voelcker
Professor
Mawson Institute
University of South Australia
Australia

ISBN 978-951-29-5185-7 (PRINT)
ISBN 978-951-29-5186-4 (PDF)
ISSN 0082-7002
Painosalama Oy - Turku, Finland 2012

Acknowledgements

In the beginning there was nothing. Then Leigh Canham said, "Let there be light!" And there was light.

My journey to the intriguing realm of porous silicon began in March 2007, when I walked into docent Jarno Salonen's office and asked him for a topic for my master's thesis. Eventually, I got quite excited about porous silicon optical filters, and ended up starting my PhD studies, in September 2008, under Jarno's guidance at the Laboratory of Industrial Physics in University of Turku. My voyage of discovery into the uncharted waters of carbonized porous filters has been far more rewarding than I had ever hoped to imagine. I would like to thank Jarno for his support, and also for giving me the freedom to conduct my own research. His extraordinary approach to science has served as a constant source of inspiration for me. Moreover, funding, which has enabled me to pay my rent, from the Academy of Finland, the Finnish Funding Agency for Technology and Innovation (Tekes), Emil Aaltosen säätiö, Turun yliopistosäätiö, and the Ministry of Education, Culture, Sports, Science & Technology in Japan (MEXT) is greatly appreciated.

The positive work environment at the Laboratory of Industrial Physics has created a pleasant atmosphere that made work almost seem like a constant holiday. For that, I have all the present and former members of the laboratory to thank. Besides actual work, I particularly enjoyed the coffee breaks and our hallway powwows. A special recognition goes to Ermei Mäkilä, who always had time to help, regardless of the matter, and who also found time for all the not-so-scientific chitchat. I am very much indebted to Professor Vicente Torres-Costa, from Universidad Autónoma de Madrid, for guiding me through my first steps when I was learning to prepare porous silicon optical filters. I was lucky enough to have his expertise at my disposal throughout the duration of my studies, and I hope that our collaboration may also continue in the future.

A large portion of the work presented in this thesis was done under the

guidance of Professor Yukio H. Ogata at the Institute of Advanced Energy in Kyoto University. Professor Ogata's kindness and compassion made my visit thoroughly enjoyable. He is truly one of a kind, and I am honoured to have been given the opportunity to work in his research group. During my 18 month stay in Japan, I met many wonderful people who helped me out tremendously. I would especially like to name Professor Tetsuo Sakka, who never ceased to amaze me with his insightful comments and suggestions. Dr. Yōichirō Suzuki's contribution proved out to be essential when I needed help with material characterization. His skill and command over the research equipment is truly phenomenal. My warmest regards also to the past and present members of the laboratory, particularly the silicon research group, namely Dr. Kazuhiro Fukami, Tomoko, Ryo, Naoto, Mitsuhiro, and Kazuki. I also want to thank all my friends in Japan, for the countless karaoke-visits, and all the fun we had together.

I would like to extend my acknowledgements to the pre-examiners of this thesis, Dr. Luca De Stefano and Professor Sharon Weiss. I humbly welcome Professor Nicolas Voelcker as my opponent. It is truly an honour. I am grateful to Dr. Robert Badeau, who provided me with excellent remarks regarding the language of the thesis, and gave me an insight on some of the more obscure grammar points. I would also like to thank all of the co-authors of my papers and everyone who have helped me with my research.

Life would be very hollow without good friends. Luckily, I have been endowed with several of them. There is not enough room to thank everyone individually, so I will settle for one huge collective Thank You. I am also fortunate to have so many wonderful relatives who have spurred me on in my studies. Special thanks to Raija and Pentti Viitanen for providing me a home away from home. Finally, I wish to express my deepest gratitude to my family. My parents Esko and Helena, who have always supported me, thank you for being the best parents one could possibly hope for. My brother Tommi, who always manages to stay cheerful, I thank you for being you.

I believe that all the work that has led to the completion of this thesis can be succinctly summarized in the words of the late Hunter S. Thompson, "If you're going to be crazy, you have to get paid for it or else you're going to be locked up."

List of Abbreviations

PSi	Porous silicon
HF	Hydrofluoric acid
SOI	Silicon on insulator
FIPOS	Full isolation by porous oxidized silicon
ELTRAN	Epitaxial layer transfer
PL	Photoluminescence
EL	Electroluminescence
EQE	External quantum efficiency
SERS	Surface enhanced Raman spectroscopy
CMOS	Complementary metal-oxide-semiconductor
DNA	Deoxyribonucleic acid
OCP	Open circuit potential
IR	Infrared
IUPAC	International union of pure and applied chemistry
TEM	Transmission electron microscopy
SEM	Scanning electron microscopy
SAXS	Small-angle x-ray scattering
AFM	Atomic force microscopy
SSA	Specific surface area
BET	Brunauer–Emmett–Teller
DMSO	Dimethylsulfoxide
TC	Thermal carbonization
THC	Thermal hydrocarbonization

DFT	Density functional theory
KOH	Potassium hydroxide
EMA	Effective medium approximation
FFT	Fast Fourier transform
TE	Transverse electric
TM	Transverse magnetic
APSFET	Adsoprtion porous silicon-based field effect transistor
PPB	Parts per billion
PPM	Parts per million
TCPSi	Thermally carbonized porous silicon
THCPSi	Thermally hydrocarbonized porous silicon
FTIR	Fourier transform infrared spectroscopy
BJH	Barret–Joyner–Halenda
GLC	Gas-liquid chromatography
FWHM	Full width at half maximum
UnPSi	Porous silicon modified with thermal hydrosilylation of undecylenic acid
UnTHCPSi	Undecylenic acid functionalized THCPSi

Contents

Abstract

In this thesis, the gas sensing properties of porous silicon-based thin-film optical filters are explored. The effects of surface chemistry on the adsorption and desorption of various gases are studied in detail. Special emphasis is placed on investigating thermal carbonization as a stabilization method for optical sensing applications. Moreover, the possibility of utilizing the increased electrical conductivity of thermally carbonized porous silicon for implementing a multiparametric gas sensor, which would enable simultaneous monitoring of electrical and optical parameters, is investigated. In addition, different porous silicon-based optical filter-structures are prepared, and their properties in sensing applications are evaluated and compared.

First and foremost, thermal carbonization is established as a viable method to stabilize porous silicon optical filters for chemical sensing applications. Furthermore, a multiparametric sensor, which can be used for increasing selectivity in gas sensing, is also demonstrated. Methods to improve spectral quality in multistopband mesoporous silicon rugate filters are studied, and structural effects to gas sorption kinetics are evaluated. Finally, the stability of thermally carbonized optical filters in basic environments is found to be superior in comparison to other surface chemistries currently available for porous silicon. The results presented in this thesis are of particular interest for developing novel reliable sensing systems based on porous silicon, e.g., label-free optical biosensors.

List of Papers

I Carbonization of porous silicon optical gas sensors for enhanced stability and sensitivity,
V. Torres-Costa, J. Salonen, *T. M. Jalkanen*, V.-P. Lehto, R. J. Martín-Palma, and J. M. Martínez-Duart, Phys. Status Solidi A **206**, 1306-1308 (2009).

II Optical gas sensing properties of thermally hydrocarbonized porous silicon Bragg reflectors,
T. Jalkanen, V. Torres-Costa, J. Salonen, M. Björkqvist, E. Mäkilä, J. M. Martínez-Duart, and V.-P. Lehto, Opt. Express **17**, 5446-5456 (2009).

III Electro-optical porous silicon gas sensor with enhanced selectivity,
T. Jalkanen, J. Tuura, E. Mäkilä, and J. Salonen, Sensor. Actuat. B **147**, 100-104 (2010).

IV Structural considerations on multistopband mesoporous silicon rugate filters prepared for gas sensing purposes,
T. Jalkanen, J. Salonen, V. Torres-Costa, K. Fukami, T. Sakka, and Y. H. Ogata, Opt. Express **19**, 13291-13305 (2011).

V Studies on chemical modification of porous silicon-based graded-index optical microcavities for improved stability under alkaline conditions,
T. Jalkanen, E. Mäkilä, Y.-I. Suzuki, T. Urata, K. Fukami, T. Sakka, J. Salonen, and Y. H. Ogata, Adv. Funct. Mater. **22**, 3890-3898 (2012).

Chapter 1

Background

1.1 Early Studies on Porous Silicon

The first report on porous silicon (PSi) was published in 1956. While investigating electrochemical methods for polishing germanium and silicon wafers, Arthur and Ingeborg Uhlir discovered that under certain conditions black, brown, or red deposits formed on anodized silicon wafers [1]. They proposed that the deposits consisted of a silicon suboxide. The discovery was made while attempting to measure the valence of the reaction. Surprisingly, a value of 2 was recorded instead of the expected value of 4 [1, 2]. Uhlir also reported hydrogen evolution at the anode, and noted that not only the color of the surface was different from polished wafers, but the electrical properties had also changed [1]. Dennis Turner conducted further experiments on electropolishing of silicon in hydrofluoric acid (HF) solutions, and found electropolishing to occur above a critical current density. Turner also suspected that anode films, formed with lower currents, might be porous, and proposed that the film is composed of a silicon subfluoride [3]. Studies on producing similar films without applied current in solutions composed of HF and nitric acid were carried out by Archer and published in 1960 [4]. In 1966, Memming and Swandt proposed a dissolution mechanism for silicon electrodes in HF [5]. They also suggested that the anode films result from a redeposition of silicon from SiF_2.

However, it was not until 1971 that Watanabe and Sakai reported the porous nature of the films formed on silicon electrodes under anodization [6]. Around the same time, Theunissen published his results on the formation of etch pits and tunnels on n-type silicon [7, 8]. After deeming the films porous, Watanabe and co-workers proceeded with investigations on utilizing oxidized PSi films in isolating bipolar integrated circuits [6, 9]. Further

experiments on the formation and thermal oxidation of PSi [10–13] laid the foundation for using the material in silicon on insulator (SOI) structures [14–18]. An example of PSi usage, in this context, is the so-called FIPOS (Full Isolation by Porous Oxidized Silicon) concept developed by Imai in the early 1980s [17]. The early work on PSi-based SOI structures culminated in the development of the epitaxial layer transfer (ELTRAN) technique [19, 20]. ELTRAN was the brainchild of Takao Yonehara, which he developed while working for Canon Inc. In this technique, an epitaxial layer is grown on top of PSi and the PSi layer is subsequently used as a sacrificial layer after wafer bonding.

The optical properties of PSi were also investigated, and, in 1984, photoluminescence (PL) under 4.2 K temperature was reported [21]. It was however Canham's paper in 1990 on visible PL at room temperature that ignited widespread interest towards PSi [22]. Around the same time Volker Lehmann and Ulrich Gösele had independently noticed that the bandgap of the material widens due to quantum confinement effects and proposed this as a plausible explanation for the formation of the porous layer [23]. However, initial rejection of their manuscript, followed by an appeal process, resulted in a delayed appearance of their paper [24]. The discovery of visible PL was soon followed by reports on electroluminescence (EL) [25–27].

1.2 Porous Silicon in Applications

After the report on visible PL by Canham [22], a huge effort was directed at explaining this phenomenon and utilizing PSi in optoelectronic applications [26–32]. Several review articles related to the subject have been published [33, 34]. Despite notable improvements in EL efficiency, a number of unresolved problems resulted in a gradual decline in interest towards the luminescent properties of PSi. For example, making good electrical contact over the surface of a PSi layer can be problematic, and poor electrical transport complicates the matter further. As a result, the external quantum efficiency (EQE) for EL turned out to be too low for practical applications [33, 35].

Fortunately, the beneficial optical properties of PSi were not limited to luminescence. In 1993, G. Vincent, working for France Telecom, filed a patent for PSi-based optical superlattices [36]. Shortly after the first reports on Bragg reflectors [36, 37], PSi-based optical microcavities [38]

and rugate filters [39] were also demonstrated. In addition, the utilization of PSi in photonic applications was further extended by electrochemically engineering two and three dimensional photonic crystals based on the material [40–44]. Interestingly, the formation of a forbidden band is not restricted to photons, but has also been observed for phonons. This can be used for creating acoustic mirrors from PSi [45–47]. PSi has also found use in other optical applications, such as photodetectors [48–50], and exhibits interesting optical properties, e.g. birefringence [51–53].

A completely new research avenue opened in 1995 when Leigh Canham reported on the bioactive nature of PSi [54]. Canham had discovered that storing PSi chips in simulated body fluid results, under certain conditions, in nucleation and growth of a hydroxyapatite layer [54]. Depending on the porosity and morphology, PSi can also be made bioinert or biodegradable [55]. These findings resulted in an increased level of interest regarding the use of the material in biomedical applications. Since then, PSi has been used, for example, as a template for cell adhesion and cell culture studies [56–58], and studied as a promising material for drug delivery applications [59–61]. In drug delivery applications, drug molecules are loaded inside the nanometer-sized pores. Among other things, the PSi-matrix protects the drugs against enzymatic degradation, and sometimes even against the natural immunological defence mechanisms of the human body, while providing a convenient means for achieving targeted delivery and biomedical imaging [60, 61]. Other examples of PSi in bioapplications include PSi-based biosensors [62–64], the use of the material for biomolecular screening [65], and as a scaffold for tissue engineering [66].

PSi can also be used as a template. The possibility of depositing polymers [67, 68] and metals [69, 70] inside PSi, enables the production of a variety of intriguing micro- and nanostructures. This has been used to create polymer replicas of optical filters [68]. Furthermore, PSi layers with noble metal particles have been used as substrates for surface enhanced Raman spectroscopy (SERS) [71–73], to name a few examples. Moreover, it has also been shown that the inclusion of noble metal nanoparticles inside a PSi matrix can induce catalytic activity [74, 75].

Studies regarding the use of PSi in gas sensing applications started to appear in the 1990s [76–80]. The large internal surface of PSi, composed of a network of nanoscale pores, promote the adsorption of gases and cause notable changes in the electrical [76–78] and optical properties [79, 80] of PSi. Especially, changes in the optical properties have also been utilized in

biosensing applications [62, 64, 81]. The simplest optical detection mechanisms are based on monitoring the changes in the reflectance spectrum or PL of a PSi thin film, but preparation of elaborate optical filters for sensing applications is also feasible [50, 80, 82, 83]. Due to compatibility of PSi with standard processes used in the integrated circuit industry, the preparation of PSi-based electrical sensing elements with readout electronics on the same chip has been proposed. This has led to the development of gas sensors with CMOS-compatible fabrication process which have been demonstrated by Barillaro et al. [84–86]. In the field of biosensing, PSi has found use in the detection of DNA, proteins, and peptides [62, 87–92]. Subsequently, the utilization of PSi-based biosensors to detect, e.g., bacteriophages [90], bacteria [93, 94], and opiates [95] has also been demonstrated.

In addition to the aforementioned applications, PSi has numerous other properties and a vast range of possible uses. Interestingly, the versatility of PSi also enables combining different applications to achieve unconventional multiparametric sensing systems.

Chapter 2

Properties of Porous Silicon

This chapter aims at giving a brief overview on the preparation and formation mechanisms of PSi produced via electrochemical anodization. In addition, other topics, such as, optical characteristics and properties related to the surface chemistry of the material are discussed. Although it is also possible to prepare PSi by other methods, such as stain etching [4, 96, 97], photosynthesis [98, 99], and metal assisted etching [100–103], these methods will not be covered here as they are not directly related to this thesis.

2.1 Preparation of Porous Silicon

Porous silicon is usually prepared by anodic dissolution of silicon wafers in HF-based electrolyte solutions. In practice, the silicon sample is placed inside an electrochemical cell together with a counter electrode and anodic bias is applied. Platinum is usually preferred as a cathode material and the electrochemical cell is composed of a material resistant to HF, such as Teflon®. Figure 2.1 depicts a commonly used design for an electrochemical cell made for the preparation of PSi. This cell, known as the o-ring cell, provides a reasonably homogeneous current density distribution across the silicon working electrode. Other type of cells such as a simple immersion cell or a more complicated double-tank cell may also be used [104–106].

In the o-ring cell design, electrical contact with the silicon electrode is provided by placing a current collector under the sample. For example, a copper plate can be used for this purpose. It is extremely important that the contact between the Si electrode and current collector be ohmic to obtain reproducible results. This can be achieved, for example, by evaporating a metal with an appropriate Fermi energy to the backside of the silicon

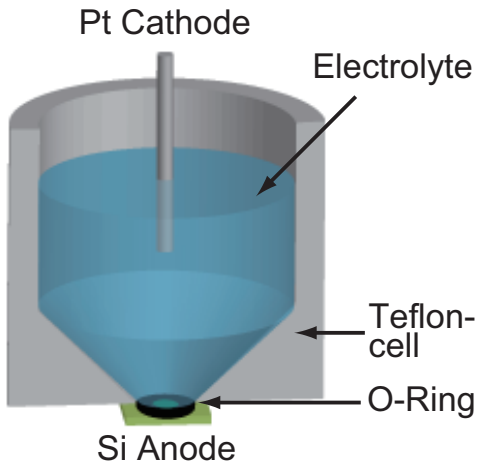

Figure 2.1: Electrochemical cell used for the preparation of porous silicon. PSi formation takes place in HF-based electrolytes when the Si electrode is under anodic polarization.

sample to produce a low Schottky barrier. For highly doped wafers with low resistivity, a simple aluminum foil back-contact is often sufficient to guarantee proper contact [105, 106]. The electrolyte solution is composed of aqueous HF and usually a surfactant, which is added to reduce the surface tension of the liquid. Ethanol is commonly used for this purpose. The surfactant allows penetration of the electrolyte inside the smaller pores and additionally aids the removal of hydrogen bubbles which are formed during the dissolution reaction [104, 107].

Porous silicon formation occurs at anodic overpotential when bias is applied between the two electrodes. Galvanostatic anodization is usually preferred over the potentiostatic one, as it allows better control over thickness and porosity of the forming layer. A characteristic current voltage curve is shown in Fig. 2.2. Above the open circuit potential (OCP), a region of exponential growth is observed. This is the region where porous silicon formation occurs [108]. PSi formation is accompanied by visible hydrogen evolution, which decreases with potential. For higher potentials, a peak in the current voltage curve is observed (J_{ep} in Fig. 2.2) which marks the transition to electropolishing regime. Beyond this peak, PSi is no longer

formed and electropolishing is the main reaction occurring at the silicon electrode. Between these two regions a transition regime exists, where the two reaction pathways compete [109]. Anodization currents in the transition region usually result in the formation of a porous layer with large pore dimensions. Well beyond the first peak, a second peak, related to the transition to current oscillation regime, appears [110]. At cathodic overpotentials, the silicon electrode is inert to dissolution and only hydrogen formation related to reduction of water can be observed at high overpotentials [105]. The exact shape and numerical values of the current voltage characteristics depend largely on experimental conditions such as the doping type and density of the Si substrate and electrolyte composition [108]. For example, for higher HF concentrations, the first peak (J_{ep}) in the I-V curve shifts to higher potential values, while for lower HF concentrations electropolishing occurs at relatively small anodization currents [109].

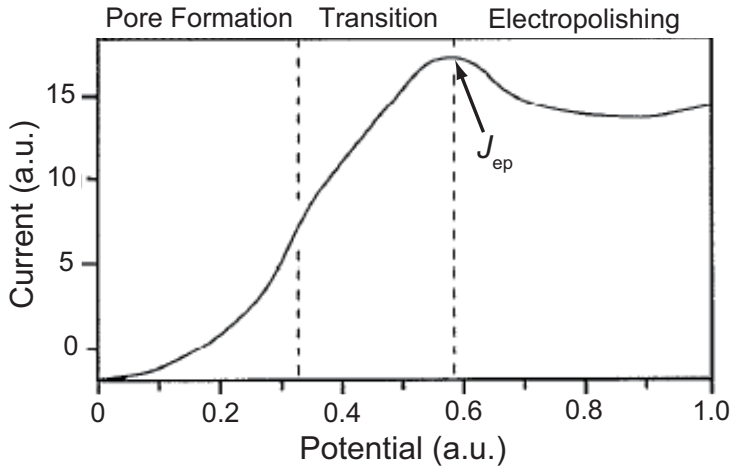

Figure 2.2: Typical I-V curve for p-type porous silicon displaying regions related to pore formation, and electropolishing. The transition region in the middle can also be distinguished clearly. Electropolishing peak (J_{ep}) marks the beginning of the electropolishing region (adopted from reference [110]).

2.1.1 Divalent and Tetravalent Dissolution

Several variants have been proposed as the main chemical reactions governing silicon dissolution in HF. Previously, it was assumed that a fluoride-terminated silicon surface would be present in HF-based electrolytes. However, IR spectroscopy revealed the Si surface to be covered with hydride species [111–113]. This holds independent of HF concentration of the electrolyte [114]. Since the Si-F bond strength ($\approx 6\,\mathrm{eV}$) is much larger than that of Si-H ($\approx 3.5\,\mathrm{eV}$), it is not plausible that hydrogen would replace fluorine on the surface during anodic dissolution. Therefore, a conclusion was made that the silicon atom must be removed from the surface upon establishing a bond with a fluorine atom. This dissolution is attributed to the strong polarizing effect caused by the fluorine atom, which exposes the back-bonds of the Si surface atoms to an attack by HF or H_2O leaving behind a H-terminated surface [105, 111, 115, 116]. Furthermore, if anodic bias is not applied, the surface is stabilized by the Si-H_x species owing to the lack of polarization of Si-Si back-bonds [115, 116].

Lehmann and Gösele have proposed a divalent dissolution mechanism for the formation of PSi (Fig. 2.3) [23, 105, 117]. Step 1 in Fig. 2.3 describes the initiation of the reaction by a hole originating from bulk Si. This results in the replacement of the hydrogen atoms on the surface by fluoride atoms. After the establishment of a Si-F bond, the second nucleophilic attack is accompanied by injection of an electron (step 2). The replaced hydrogen escapes as gaseous H_2, while the fluoride-terminated silicon atoms react with HF breaking the silicon back-bonds (steps 3 and 4). After the dissolution, the remaining silicon surface is terminated with hydrogen (step 5). Similar reaction schemes with slight differences have also been proposed by other research groups [118–120].

As we can see from the dissolution mechanism described above, a basic requirement for the formation of PSi is the availability of holes [116]. For *p*-type silicon, positive charge carriers are supplied by the doping material, and thus PSi formation occurs when anodization current is applied. However, for non-heavily doped *n*-type Si, much larger potentials are required to initiate the dissolution reaction in the dark [121]. In this case, holes are generated when breakdown voltage is reached [122]. The shape of the *I*-*V* curve for *n*-type silicon largely depends on the lighting conditions, and holes may also be supplied by illumination during anodization [105, 109, 122–124]. The pore walls in PSi are depleted of charge carriers and thus the

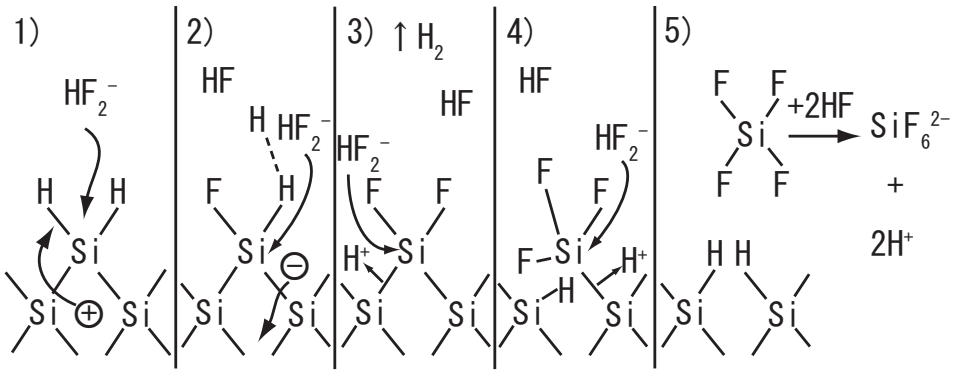

Figure 2.3: Reaction scheme proposed for the anodic divalent dissolution of Si electrodes in HF [23, 105].

active reactions only occur at the pore tips [116].

For anodization currents past the electropolishing peak (J_{ep}), the dissolution mechanism changes distinctly. As the anodization current values increase, the diffusion of HF to the electrolyte electrode interface will become the rate limiting factor [105]. This results in the formation of an anodic oxide layer at the pore formation front. The high potential enables OH^- to diffuse through the oxide film and establish a Si-O-Si bridge [105, 125]. The oxide layer then dissolves in HF. The reaction responsible for electropolishing is termed tetravalent dissolution. The existence of an oxide layer during PSi formation has also been confirmed experimentally [126]. Moreover, the electropolishing region does not occur in anhydrous organic solutions due to the lack of water required to form the oxide layer [116]. The electropolishing reaction may be used for detaching PSi layers from the silicon substrate to form free-standing PSi films [106]. The dissolution valences for the idealized reactions presented above are 2 and 4, respectively. Effective dissolution valences measured for PSi formation depend on the experimental conditions and usually vary between 2 (pore formation) and 4 (electropolishing) [116]. In general, the dissolution valence increases with current density, and decreases with growing PSi layer thickness [116, 127]. For thick films, values below 2 are observed, which can be attributed to the slow chemical dissolution of PSi in the electrolyte solution.

2.2 Structure and Morphology of Porous Silicon

Structure and morphology of PSi is greatly dependent on the formation parameters, such as doping type and dopant concentration of the Si substrate, illumination conditions, electrolyte composition, temperature etc. [109, 128, 129]. Classification of different types of PSi layers is primarily done according to pore sizes. For p-type Si, the pore diameter generally increases with doping concentration, whereas for n-type Si, it decreases with doping concentration. Pore sizes also increase as the anodization potential or current density is raised but decrease if the HF concentration of the electrolyte is increased [109]. Pore sizes are usually divided into micro-, meso-, and macropores according to the pore diameter. This is based on the classification of pore sizes by the International Union of Pure and Applied Chemistry (IUPAC), which is presented in table 2.1 [130]. Experimental determination of pore sizes can be accomplished for example with nitrogen sorption [131–133], transmission electron microscopy (TEM) or scanning electron microscopy (SEM) [106, 133–136], and small-angle x-ray scattering (SAXS) [137, 138]. In some cases, atomic force microscopy (AFM) can also be useful for determining pore sizes on the surface [63]. It is important to keep in mind that methods based on microscopic imaging only allow the localized determination of pore sizes in the observed area [133].

Due to large variation in PSi morphology, the IUPAC classification alone does not adequately describe the porous structure. Usually a layer of PSi is composed of a distribution of different pore sizes, rather than pores of a certain fixed diameter. In general, the primary pores in micro- and meso-PSi show various degrees of branching into smaller side pores [116]. The degree of branching increases as the anodization current density in decreased leading to "spongy" or "fir tree"-like morphologies. Figure 2.4 presents some of the numerous morphologies that can be produced from p-type silicon.

The type and concentration of the dopant have a large effect on the size and morphology of the pores formed. Moderately doped p-type Si can be used to produce PSi with small pore sizes in the range of 1-10 nm. For highly doped p and n-type substrates pore diameters are usually in the range of 10-100 nm. Wide range of pore diameters from micropores to 10 μm, are obtainable with n-type silicon. Illumination conditions also have a large effect on the morphology of PSi formed on n-type substrates. Micro- and macropores may be observed for p-type substrates with low doping concentration. One sample can also contain two size distributions

with a crust of micropores on top of a macroporous layer or a layer of macropores that are partially or fully filled with micropores [109, 116, 139, 140]. Two size distributions of pores have also been observed for n-type silicon [141, 142].

Table 2.1: Classification of pore sizes according to IUPAC

Type of pore	Pore width [nm]
micro	< 2
meso	2 - 50
macro	> 50

In addition to pore size, porosity and the specific surface area (SSA) are often useful parameters in characterizing the porous structure. Porosity is the fraction of void in the porous layer, and it is therefore not related to the pore diameter. Porosity can be determined easily with the gravimetric technique by measuring the weight of the sample before and after the anodization, and finally after the porous layer has been dissolved from the substrate [144]. Specific surface area is an important parameter in sensing applications along with the pore diameter. Determination of the SSA can be accomplished by employing the BET (Brunauer-Emmett-Teller) method [145] to the adsorption isotherms of gases such as nitrogen [132, 146, 147]. Surface areas measured for highly doped p-type silicon are usually in the range of $200\,\mathrm{m}^2/\mathrm{cm}^3$, but for lightly doped samples the SSA values can be several times larger [133, 147, 148].

The shape of individual pores can vary among different anodization conditions. The shapes can be roughly grouped into round, square-shaped, star-shaped, and dendritic pores [116, 149]. Triangular pores have also been reported for macroporous silicon [140]. Pore growth is anisotropic, i.e. the pores tend to grow toward the $\langle 100 \rangle$ crystallographic direction or along the primary field lines [109, 150, 151]. When (100) substrate is used, the orientation of primary pores is in the $\langle 100 \rangle$ direction independent of anodization parameters [116]. In the case of some dendritic structures, preferential propagation of pores along the $\langle 100 \rangle$ direction is observed even for (110) and (111) substrates [149, 151, 152]. Branched pores may deviate

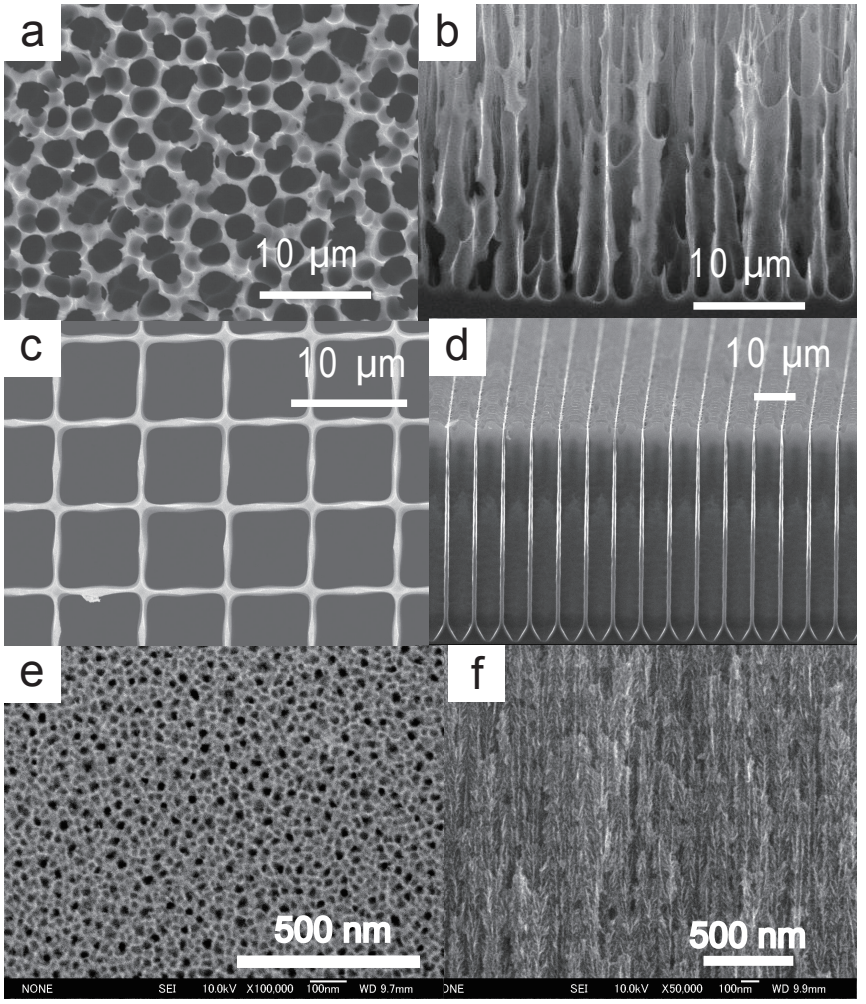

Figure 2.4: SEM micrographs demonstrating the different pore sizes and morphologies obtainable with *p*-type silicon. Plan view of macroporous silicon produced on lightly doped polished (a) and pre-patterned (c) (100) oriented substrates. Cross-sectional view of macroporous silicon for polished (b) and pre-patterned (d) wafers [143]. Plan view (e) and cross-section (f) of mesoporous silicon anodized on a heavily doped *p*-type wafer (unpublished results).

to various degrees from the ⟨100⟩ direction towards the direction of holes. It has also been reported that under certain anodization conditions pores oriented in the ⟨113⟩ direction may form [153–156].

2.3 Formation Models

Several models have been proposed to describe the formation of PSi. However, due to the rich morphology and wide range of feature sizes present in different types of PSi, a model that would comprehensively explain PSi formation does not exist. Nevertheless, some models have been fairly successful in explaining the phenomenon under certain conditions with some limitations in the scope and validity of the respective models. A brief description of the most important models will be provided here.

The first model that provided a rather extensive explanation was proposed by Beale et al. [135]. They noticed that the porous layer was highly resistive and therefore suggested that the pore walls are depleted of carriers. TEM measurements also revealed that the separation between pores is always less than the width of the depletion layer. They postulated that surface defects at the silicon electrolyte interface result in a high density of surface states and consequently in the pinning of the Fermi level near mid-gap. Since the PSi layer is depleted of carriers, the current is localized at pore tips [134, 135]. The initiation of pores was attributed to random inhomogeneities in the current flow at the interface [135].

Smith et al. explained the formation of PSi and the resulting morphology based on the hypothesis that the rate of growth is limited by the diffusion of holes from the bulk of the semiconductor to the pore tips at the formation front [110, 157]. In this diffusion limited model, the movement of holes from the bulk toward the porous layer is described as random walk [157]. According to the model, silicon is dissolved as the holes make contact with the pores. As a result of the random nature of hole diffusion, the holes are more likely to make contact with pores nearest to them. Thus the outermost tips of the pores, close to the diffusion surface, have the highest probability of capturing the holes and growing. The hole diffusion length, which is a function of potential and dopant concentration, essentially determines the morphology of the porous layer [157]. Computer simulations on the morphology of PSi agree well with experimental findings under certain experimental conditions [110, 158]. The model avoids some of the assump-

tions made by the Beale model, such as Fermi level pinning. However, the differences between the two models are not that significant, and actually the models are mathematically equivalent. Therefore, exactly the same morphology simulated with the diffusion limited model could also be generated with the Beale model [110]. The diffusion limited model is too general to account for the different current conduction mechanisms for different types of silicon substrates, and thus can not explain all the experimentally observed morphologies [116]. Moreover, on the basis of more recent experimental results regarding hole diffusion into the Si skeleton, the random walk approach seems rather unrealistic for describing hole accumulation to the pore tips.

In the early 1990s, Lehmann and Gösele proposed that formation of micropores can be explained by quantum confinement effects [23, 117]. The band-gap energy in the PSi layer increases as the pore walls become thinner. This leads to an energy barrier which prevents the charge carriers from entering the pore walls. As a result, the pore walls are depleted of carriers and the porous layer is passivated against further dissolution. Frohnhoff et al. later expanded the model to account for the wide distribution of pores found in PSi formed on *p*-type substrates [159]. The quantum model does not provide an explanation regarding the factor that determines the pore size.

More recent and perhaps the most comprehensive model, on the formation of different types of PSi, is the current burst model [160–164]. The model assumes that current flow occurs by local current bursts. Current flow induces either direct dissolution or oxide formation and dissolution which always follows a current burst. The hydrogen termination process is an important contributing element to the current oscillations. The problem with this kind of unified model is that it is extremely difficult to express in mathematical form because it needs to account for all the observed phenomena [116].

2.4 Methods for Chemical Modification

As it was noted in section 2.1.1, the divalent dissolution reaction results in a hydrogen terminated surface. Therefore, freshly prepared PSi surface is covered with hydride species, which has also been confirmed experimentally [165–167]. The existence of hydrogen termination has also

been observed in situ during fabrication [168]. Already in 1965, Beckmann noted that the composition of PSi slowly changes in ambient air [169]. During the 1990s, it was established that these changes were caused by oxidation of the hydrogen terminated surface, and that the oxidation has pronounced effects on the electrical, optical, and structural properties of the material [170, 171]. Similarly to non-porous Si surfaces [172], the rate of oxidation for PSi is largely dependent on the storage conditions. For example, decomposition of water upon adsorption has been observed [173], and can be attributed to the fact that both Si-Si and Si-H bonds are able to reduce water [106]. The slow oxidation of PSi in ambient atmospheric conditions is therefore accelerated under humid environment [174–176]. Rate of oxidation is also greatly affected by the type of the PSi layer and the substrate [177, 178].

The atmospheric oxidation of PSi is especially problematic for many applications. For example, the luminescent properties of PSi change as the surface undergoes oxidation [170, 179–181]. In sensing applications gradual oxidation leads to a baseline drift of the sensor. For instance, the high sensitivity reported for a PSi-based biosensor [62] was later explained with the oxidation of PSi in aqueous solutions [87]. Fortunately, many strategies have been developed to stabilize the surface of PSi, and some of them will be presented below.

2.4.1 Oxidation

One of the simplest and most effective ways to passivate the surface of freshly prepared PSi is to deliberately oxidize it. Thermal oxidation has been studied since the 1970s, when the use of PSi as an isolation material for integrated circuits was first discovered [9, 12]. Many parameters affect the outcome of the thermal oxidation process, such as the treatment temperature and time, and also the humidity of the ambient atmosphere [106]. For example, rapid thermal oxidation for 30 s has been proven to result in a high quality oxide surface that is stable under ambient conditions [182]. Temperature of the oxidation treatment has an effect on the type of oxide formed [183, 184]. For *p*-type silicon, at temperatures around 200 °C the surface hydrides are not replaced by oxygen, but the oxidation proceeds through back-bond oxidation of the silicon atoms [166]. When the temperature is raised near 250 °C, the surface hydrides start to convert to Si-OH species [166, 183]. At lower temperatures (200-400 °C) saturation in the

degree of oxidation is observed. The reaction that takes place at lower treatment temperatures has a lower activation energy, and is associated to the oxidation of the pore walls [184]. For higher temperatures ($> 600\,^{\circ}\mathrm{C}$), complete conversion to SiO_2 may be observed. The time needed to completely transform the structure to silica depends on treatment temperature and morphology of the PSi film, i.e. porosity etc. [184]. Two oxidation reactions have also been observed for PSi formed on n-type silicon, but the activation energies for the reactions are slightly different. This observation was attributed to differences in the internal surface of PSi prepared on p and n-type substrates [185]. Thermal oxidation causes structural changes in the PSi layer [186]. For example, pore diameter and porosity usually decrease due to volume expansion as the Si pore walls are converted to SiO_2 [187], but an expansion in the average pore diameter may also result due to annealing effects [188]. A drastic reduction in surface area occurs for temperatures beyond $600\,^{\circ}\mathrm{C}$ [55]. As a result of oxidation, the optical refractive index of PSi decreases, as does the optical absorption co-efficient [187].

Other oxidation methods, such as electrochemical and chemical oxidation, have also been studied [189]. Electrochemical oxidation is based on the fact that it is possible to grow oxide layers on silicon electrodes via anodization in alkaline electrolytes or in acidic electrolytes free of HF [105]. The same method may also be applied to PSi [190–192]. The problem with this method is that the PSi layer is usually not completely passivated because the electrical contact between the silicon electrode and the electrolyte becomes short-circuited by the growing oxide layer at the pore tips [190]. Chemical oxidation is a simple method that can be accomplished by subjecting PSi to an oxidizing agent such as dimethylsulfoxide (DMSO) [193], pyridine [194], ozone (O_3) [195], or hydrogen peroxide (H_2O_2) [195]. In general, the best results in terms of oxide surface coverage, are usually obtained by combining different oxidation methods, such as thermal and chemical oxidation [188]. For example, high-pressure water vapor annealing has been proved to result in a fairly stable oxide passivation [196–198].

2.4.2 Organic Derivatization Through Si-C Bonds

In the beginning of the 1990s, the stability of Si-C bonded species on single crystalline surfaces was recognized [199, 200]. Soon after, the same idea was applied to PSi. Some of the early approaches used aryllithium [201] and Grignard [202] reagents for cleaving Si-Si bonds on PSi surface, and conse-

quently attaching organic moieties to the surface through Si-C bonds [203]. The group of Jillian Buriak demonstrated successful functionalization of the PSi surface with alkenes and alkynes with a hydrosilylation reaction [204, 205]. They presented a Lewis acid mediated approach [206, 207] and a white-light induced, i.e. photochemical, approach [208, 209] for hydrosilylation. The white-light induced reaction also enables photopatterning on the PSi surface. At the same time, reports on thermally promoted hydrosilylation of alkenes and alkynes also started to appear [210–212]. Thermal hydrosilylation is a simple approach where the PSi sample is covered with the reagent and simply heated under Schlenk-line conditions for several hours. Boukherroub and co-workers also demonstrated thermal hydrosilylation of undecylenic acid with PSi, which resulted in a hydrophilic surface [213]. The carboxylic acid functional group on the derivatized PSi surface can be further transformed to a succinimidyl ester, which makes the thermal hydrosilylation treatment a very attractive option for biosensing applications [213]. In addition, the treatment efficiency in the thermal hydrosilylation reaction is higher in comparison to a similar reaction under catalytic conditions [207, 211]. Microwave-assisted hydrosilylation is another convenient method, which has been demonstrated to increase the reaction rate and treatment efficiency [214].

However, in all the treatments presented above, the surface is merely decorated with the functional group and left with a partial hydrogen termination, which is due to steric hindrance caused by the organic molecules on the surface [106, 212, 215]. Lees et al. have reported an interesting two-step method for improving surface coverage of a functionalized PSi surface [216]. They used reductive coupling of iodomethane for electrochemically endcapping most of the remaining Si-H sites on the PSi surface, which resulted in significant improvements in stability.

2.4.3 Thermal Carbonization

Adsorption and thermal decomposition of acetylene on single-crystalline Si surfaces has been the subject of many studies in the past [217–221]. Due to the high activation energy for desorption, the chemisorbed acetylene molecules undergo decomposition upon heating with subsequent H_2 desorption [220]. Only a small fraction of the surface species desorb as intact C_2H_2 molecules. Interestingly, this behaviour is in stark contrast to thermal desorption of ethylene (C_2H_4), for which approximately 98 % of

the chemisorbed molecules desorb without decomposition [220]. When the acetylene covered surface is heated above 660 °C, hydrogen atoms desorb from the surface and carbon atoms bind to the Si surface. In addition, carbon atoms penetrate into the Si bulk immediately after the beginning of H_2 desorption [220, 221].

The same approach can also be used for stabilizing the surface of PSi, as demonstrated by Salonen [222–224]. This method is referred to as thermal carbonization (TC), and it results in efficient passivation of the PSi layer. The treatment can be divided in two sub-categories, namely thermal carbonization and thermal hydrocarbonization (THC). The THC treatment takes place at temperatures below 660 °C thus leaving hydrogen atoms on the surface [224]. In THCPSi, the carbon atoms do not penetrate into the Si bulk, but instead hydrocarbon species bind on the surface. Experimental results and density functional theory (DFT) calculations show that there are several plausible binding configurations for the hydrocarbon species [224], and therefore the THC treatment does not result in a simple monolayer coverage in the same way as many of the organic derivatization techniques.

Lower temperatures used in the THC treatment also enable the use of continuous acetylene flush during the heat-treatment, thereby increasing treatment efficiency [224]. This aspect can be utilized also in the high temperature TC treatment by performing a pre-THC treatment to improve surface coverage and stability [225]. Unlike the C_xH_y-covered surface found in THCPSi, in TCPSi, the hydrogen atoms are removed from the surface and carbon is incorporated into the Si skeleton [223]. Additionally, the outer surface of the TCPSi is capped with a thin oxide layer [226]. These differences in the respective surfaces result in remarkable changes in hygroscopic character of the material [224, 227]. Similarly to as-anodized PSi, the THCPSi surface remains hydrophobic, while the TCPSi surface is very hydrophilic. The degree of affinity towards humidity can be controlled by adjusting the preparation parameters [228].

The carbonization treatment has been shown to increase the electrical conductivity of PSi films [229]. This behaviour accompanied with the increased stability and a relatively small decrease in the specific surface area, make carbonized PSi a promising material for sensing applications [222, 223]. Consequently, TCPSi humidity sensors based on monitoring the electrical changes have been demonstrated [230–232]. In addition, in a study comparing the stability of different surface treatments of PSi for

sensing applications, TCPSi was found to be extremely stable in environments such as KOH [233]. Recently, studies regarding the functionalization of THCPSi have also been published [234, 235]. This opens new possibilities for utilizing the carbonization treatment in biosensing applications.

2.5 Refractive Index

In general, the refractive index ($\boldsymbol{n}$) of a dielectric is defined by the ratio of velocity of light in free space and velocity of light in the medium [236, 237]. Moreover, the refractive index is composed of a real and imaginary part and can be presented as:

$$\boldsymbol{n} = \frac{c}{v} = n + \mathrm{i}k, \tag{2.1}$$

where c and v are the speed of light in vacuum and in the material, respectively, and n and k are the real and the imaginary part of the refractive index. The imaginary part of the refractive index k, also known as the extinction coefficient, is related to absorption of light in the incident medium [236]. In an absorbing medium, the intensity of incident light falls exponentially as a function of distance travelled [238].

The refractive index can also be expressed in regard to relative permittivity ϵ_r and relative permeability μ_r, where:

$$\boldsymbol{n} = \sqrt{\epsilon_r \mu_r}. \tag{2.2}$$

However, when ferromagnetics are excluded, μ_r can be considered unity, and thus we end up with an approximate relationship, where $\boldsymbol{n}^2 = \epsilon_r$. One should keep in mind that both the refractive index and also the relative permittivity depend on the wavelength of light, in other words, they are frequency dependent. Thus we can write the following expression describing the dielectric function:

$$\varepsilon(\omega) = (\boldsymbol{n}(\omega))^2, \tag{2.3}$$

which is in good agreement for non-polar substances [239].

The reported refractive index values for PSi differ from those of bulk Si [21, 50]. In addition to the real part of the refractive index, a decrease in the absorption coefficient, as demonstrated by a shift in the absorption

edge, is also observed [23, 240, 241]. In order to understand the effect that porosity has on the refractive index of PSi, we need to consider the concept of refractive index for a porous solid. We can think of PSi as a mixture of silicon and voids that are filled with the ambient medium, which is, in most cases, air. For micro- and mesoporous silicon the size of the pores is significantly smaller than the wavelength of visible light. Therefore, from an optical point of view, we can consider certain type of PSi as a homogeneous mixture of silicon and air. The effective refractive index and dielectric function of such a material can be described with so-called effective medium theories [242, 243]. In theory, by controlling the porosity, we can adjust the refractive index of PSi resulting in values between those corresponding to refractive indices of air and silicon. In practice, the range of obtainable values is limited by the porosity values that can be experimentally produced [50].

Several effective medium models have been presented, with the most prominent ones being those of Maxwell-Garnett [244], Bruggeman [245], and Looyenga [246]. Bergman [247] has also derived a general expression for the effective dielectric function:

$$\varepsilon_{\mathrm{eff}} = \varepsilon_{\mathrm{M}} \left(1 - (1-p) \int_0^1 \frac{g(n,p)}{\frac{\varepsilon_{\mathrm{M}}}{\varepsilon_{\mathrm{M}}-\varepsilon} - n} dn \right), \tag{2.4}$$

where ε_{M} is the dielectric function of the matrix material (in our case Si), p is the porosity i.e. fraction of void, $g(n,p)$ is a spectral function describing the geometry of the system, and ε is the dielectric function of the embedded material [242]. Since this expression is general, with the appropriate choice of a spectral function, any effective medium approximation (EMA) can be represented [242].

Effective dielectric function of PSi is most often modelled with the Bruggeman EMA. The following equation is used for describing the Bruggeman model:

$$p \frac{\varepsilon_{\mathrm{M}} - \varepsilon_{\mathrm{eff}}}{\varepsilon_{\mathrm{M}} + (d-1)\varepsilon_{\mathrm{eff}}} + (1-p) \frac{\varepsilon - \varepsilon_{\mathrm{eff}}}{\varepsilon + (d-1)\varepsilon_{\mathrm{eff}}} = 0, \tag{2.5}$$

where d is the dimensionality of the system. In most cases, the term $(d-1)$ is given a value of 2. Popularity of the Bruggeman EMA is in part due to studies on amorphous silicon surfaces conducted by Aspnes et al., which revealed that the Bruggeman model gave the best fit to experimental data [248]. As

the effective dielectric function of PSi depends on the material embedded in the silicon matrix, we notice that the value changes if the pores are completely filled with a substance that has a dielectric function different from that of air. Moreover, if the pores are only partially filled with a substance the Bruggeman expression can be extended to account for three components, namely Si, air, and the third substance partially filling the pores [249].

2.5.1 Determination of Optical Constants for PSi

As we have just mentioned above, the refractive index of PSi can be calculated by using the Bruggeman EMA, provided that we have a value for the porosity. Porosity can easily be determined with the gravimetric method [132], giving us a simple means for determining the refractive index of a PSi layer. However, the accuracy of this method is limited by experimental error, and simplifications used in the EMAs. For more accurate results, the refractive index and the extinction coefficient of a PSi layer may be determined with ellipsometry [250, 251], or numerically from the reflectance spectrum [252]. In the latter method, a calculated reflectance spectrum is compared to a spectrum that has been experimentally determined for a PSi thin film. Numerical methods for optimizing the theoretical spectrum are used, and the optical constants are obtained from the spectrum that gives the best fit to the experimental data [252]. The theory needed for calculating a reflectance spectrum is explained briefly in the following section 2.5.2.

The real part of the refractive index can also be determined simply from the position of successive interference fringe maxima or minima observed in the reflectance spectrum of a PSi thin film, using the following expression:

$$\frac{1}{2nd} = \frac{1}{\lambda_m} - \frac{1}{\lambda_{m+1}}, \tag{2.6}$$

where d is the thickness of the thin film, and λ_m and λ_{m+1} are the wavelength positions of the successive interference fringe maxima or minima [253]. However, the above expression is approximate and does not take absorption and dispersion into account [21]. Therefore it is only valid in the infrared region, where absorption and dispersion are usually negligible. It should be noted though that, in some cases, effects related to Si crystallite size and free carrier absorption can be significant also in the infrared region [254].

Refractive index of PSi has also been evaluated using other methods, such as dispersive Fourier transform spectroscopy [255], and the envelope method [256–258]. The group of Prof. Michael Sailor has used a fast Fourier transform (FFT) algorithm for determining the optical thickness of a PSi thin film from the reflectance spectrum [106].

2.5.2 Thin Film Reflectance

The equations needed for calculating the reflectance spectrum of a thin film are presented below. For the sake of brevity, the main results are given here without proof. The enthusiastic reader is encouraged to consult the books by MacLeod [236], and Born and Wolf [237] for a rigorous treatment.

Upon contact with a smooth interface of an absorbing medium light is either reflected, transmitted, or absorbed. Therefore for reflectance R, transmittance T, and absorptance A it must be that:

$$R + T + A = 1. \tag{2.7}$$

Moreover, the reflectance for a dielectric thin film can be calculated according to the following equation:

$$R = \left(\frac{\eta_0 B - C}{\eta_0 B + C}\right)\left(\frac{\eta_0 B - C}{\eta_0 B + C}\right)^{*}. \tag{2.8}$$

The term η_0 is the modified optical admittance of the surrounding medium, and the terms B and C are defined by the following matrix:

$$\begin{pmatrix} B \\ C \end{pmatrix} = \begin{pmatrix} \cos\delta & (\mathrm{i}\sin\delta)/\eta \\ \mathrm{i}\eta\sin\delta & \cos\delta \end{pmatrix}\begin{pmatrix} 1 \\ \eta_s \end{pmatrix}, \tag{2.9}$$

where δ is the phase change introduced by the layer, and η and η_s are the optical admittances of the layer and the substrate, respectively. The phase change is given by the expression:

$$\delta = \frac{2\pi \boldsymbol{n} d\cos\theta}{\lambda},$$

where d is the thickness of the layer and θ is the angle of incidence. The optical admittance is $\eta = \mathscr{Y}\boldsymbol{n}\cos\theta$ for s-polarized (TE) and $\eta = \mathscr{Y}\boldsymbol{n}/\cos\theta$ for p-polarized (TM) light, where $\mathscr{Y}$ is the optical admittance in free space

defined as $\mathscr{Y} = (\varepsilon_0\mu_0)^{1/2}$. We can easily extend this result to account for a stack of q thin films, which results in the following expression:

$$\begin{pmatrix} B \\ C \end{pmatrix} = \left(\prod_{r=1}^{q} \begin{pmatrix} \cos\delta_r & (\mathrm{i}\sin\delta_r)/\eta_r \\ \mathrm{i}\eta_r \sin\delta_r & \cos\delta_r \end{pmatrix} \right) \begin{pmatrix} 1 \\ \eta_s \end{pmatrix}, \tag{2.10}$$

where $\delta_r = 2\pi \boldsymbol{n}_r d_r \cos\theta/\lambda$. This result combined with equation 2.8 allows us to calculate the reflectance for a dielectric multilayer stack.

2.6 Porous Silicon Optical Filters

Two interesting properties in particular make PSi an intriguing material for optical filter preparation. The first one is the possibility to lower the refractive index of a PSi layer by increasing the porosity. The second interesting property, enabling filter preparation, is the fact that temporal changes in the anodization conditions only cause changes at the pore formation front. In other words, modifying, for example, the anodization current, does not affect the properties of the porous layer that has already been formed. The reason for this peculiar behaviour is that the dissolution process requires positive charge carriers in order to proceed, as discussed in section 2.1.1. Therefore, as the Si skeleton in the already formed PSi-layer is depleted of charge carriers, the layer is inert to further dissolution. As a consequence, any temporal changes in anodization conditions only affect the porosity and pore size of the layer forming below the already anodized layer. This enables facile production of dielectric multilayer stacks, by, e.g., modulating the anodization current as a function of time.

2.6.1 Discrete Multilayer Structures

The simplest optical filter structure is called a distributed Bragg reflector, which consists of a periodic stack of two alternating layers, with distinct refractive index values, both fulfilling the Bragg condition:

$$nd = \frac{\lambda_0}{4}, \tag{2.11}$$

where n and d are the refractive index and thickness of a layer, and λ_0 is the resonant wavelength. A structure corresponding to a Bragg reflector consisting of m bi-layers, where H represents the high refractive index (n_H)

layer and L the low refractive index (n_L) layer, can be expressed compactly as:

$$HLHLHL...HL = (HL)^m. \tag{2.12}$$

The Bragg reflector displays a broad reflective band, known as a stopband, centered at the resonant wavelength λ_0. A simulated spectrum for a Bragg reflector is shown in Fig. 2.5 (a). The first Bragg reflectors based on PSi were demonstrated in the early 1990s [36, 37].

A Fabry-Pérot filter, also known as an optical microcavity, can be fabricated easily by disrupting the periodicity of the Bragg stack by changing the stacking order to:

$$HLHL...HLLH...LHLH = (HL)^{m/2}(LH)^{m/2}. \tag{2.13}$$

The introduction of a thicker layer in the middle of the structure creates a resonant optical cavity. This causes a sharp transmission band to appear in the middle of the reflective stopband (Fig. 2.5 (b)). Optical microcavities based on PSi have also been demonstrated by several groups [38, 129, 259, 260]. Optical microcavities also enable the production of several narrow transmission bands into the reflective stopband. This can be done either by fabricating a thick cavity layer that has several resonant modes inside the stopband, or by splitting the cavity mode by preparing coupled cavity layers [261]. More complex aperiodic structures, such as Fibonacci and Thue-Morse type multilayers, may also be created from PSi [262–265]. The layer ordering in these dielectric thin film assemblies is generated with a corresponding deterministic rule.

2.6.2 Rugate Filters

The interference filters described in the previous section were based on stacking discrete dielectric layers on top of each other. However, it is also possible to induce similar interference effects by allowing the refractive index of a layer to vary continuously as a function of layer thickness in a periodic manner. Such periodic inhomogeneous layers are sometimes referred to as rugate filters [266, 267]. In order to produce a rugate filter with a stopband centered at λ_0, the following refractive index profile can

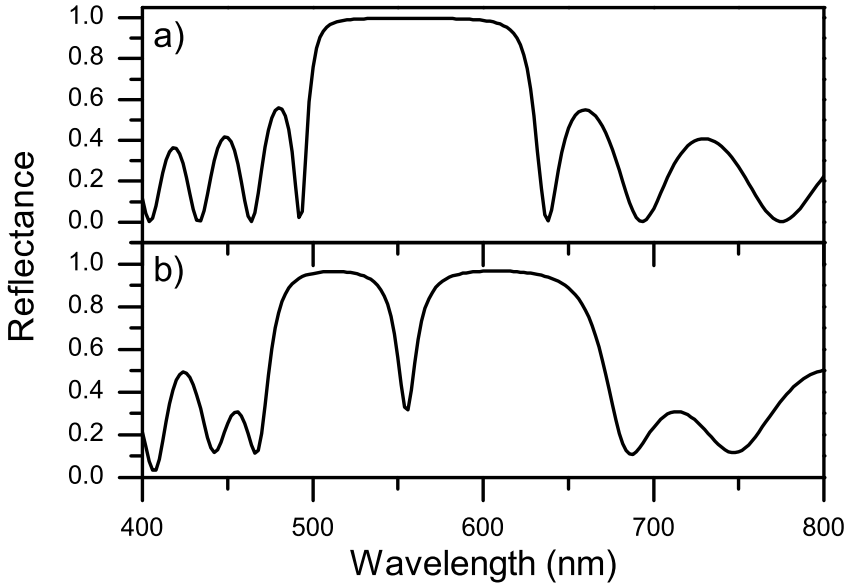

Figure 2.5: Reflectance spectra for a Bragg reflector (a) and a Fabry-Pérot microcavity (b) simulated with the transfer matrix method. The spectra were simulated with $n_H = 2.3$, $n_L = 1.7$ and $\lambda_0 = 550\,\text{nm}$. The stacking order was according to equations 2.12 and 2.13, where $m = 10$. Dispersion and absorption were not taken into account.

be applied:

$$n(z) = n_a + \frac{n_H - n_L}{2} \sin\left(\frac{4\pi z}{\lambda_0}\right), \tag{2.14}$$

where z is the distance perpendicular to the filter surface, n_a is the average refractive index ($n_a = \frac{1}{2}(n_H + n_L)$), and n_H and n_L are the maximum and minimum values for the refractive index variation [268, 269]. This type of a refractive index profile is easy to approximate with PSi by modulating the anodization current sinusoidally. Moreover, it is also possible to take into account the slight variations in the layer formation speed for different current densities in order to get a true sinusoidal refractive index variation [270].

A distributed Bragg reflector will display higher order harmonics in

the reflectance spectrum. A rugate filter, produced with the sinusoidal refractive index variation presented above, is also expected to have higher order peaks with a smaller amplitude. The high-order harmonics can be suppressed by modulating the logarithm of the index profile as follows [266, 269]:

$$\ln\left(n(z)\right) = \frac{\ln n_H + \ln n_L}{2} + \frac{\ln n_H - \ln n_L}{2} \sin\left(\frac{4\pi z}{\lambda_0}\right). \tag{2.15}$$

First rugate filters based on PSi were demonstrated by Berger et al. in 1997 [39]. Filters displaying multiple stopbands may also be accomplished easily by using a refractive index profile consisting of several sinusoidal waves in superposition [266]. These type of rugates have also been prepared from PSi by several research groups [39, 269, 271]. Another way for achieving multiple reflective bands is by placing filters in series, i.e. by stacking them on top of each other [65, 266]. Rugate filters also allow for other interesting techniques such as sidelobe suppression which can be accomplished with the use of apodization functions [272, 273] or by including refractive index matching layers at filter interfaces [274]. These techniques have also been successfully implemented in PSi-based rugate filters [39, 253, 269, 275].

2.7 Porous Silicon in Sensing Applications

The large internal surface area, adjustable pore size distribution, and compatibility with existing silicon-based technologies make PSi an extremely versatile material for a myriad of environmental and chemical sensing applications. In recent years, PSi has found use in such rapidly developing fields as biosensing [64, 276], but here we will mainly focus on gas sensing applications [277].

Gas sensing with PSi is based on adsorption. Adsorption, in general, can be divided to physisorption and chemisorption. In most cases, chemisorption is not desired since it leads to irreversible changes and can only be utilized in disposable sensors where regeneration of the sensing capabilities might be difficult or impossible to achieve. For a mesoporous material, capillary condensation also needs to be taken into account. Capillary condensation is described by the Kelvin equation, which for cylindrical pores

takes the following form:

$$r_K = -\frac{2\gamma V_m \cos\theta}{RT\ln(p/p_0)}, \tag{2.16}$$

where r_K is the Kelvin radius, γ is the surface tension of the liquid, V_m the molar volume of the adsorbate, θ is the contact angle between the solid and condensed phase, R is the universal gas constant, T is temperature, and p and p_0 are the vapor pressure and saturated vapor pressure, respectively [278]. For a certain value of pressure, gas will condensate inside all pores with a radius smaller than or equal to the radius given by the Kelvin equation. In most cases, the cosine term related to the contact angle θ is given a value of 1.

Adsorption of vapors inside the porous layer changes the electrical and optical properties of PSi. This enables us to detect variations in the composition of the ambient atmosphere by monitoring the changes in the electrical or optical characteristics. There are several ways to achieve this, and some of these detection schemes will be reviewed here.

2.7.1 Electrical Sensing

Fabrication of electrical contacts is a prerequisite for measuring the electrical characteristics of a PSi layer. Different electrode configurations have been used for PSi and the electrode placement and geometry also have an impact on the sensitivity and reproducibility of the measurement. Simple parallel electrodes are often used, but sensitivity may be increased by using a more complicated interdigitated electrode design. The electrodes are often patterned on top of the PSi surface [230, 279], but other configurations may also be used. Other designs include a sensor where one electrode is on the surface and the second one is on the bottom of the Si substrate [77], and a sensor that has two electrodes on the bottom of the substrate [280]. It is also possible to use a three terminal configuration, where two electrodes are located on the top-surface and one is at the bottom of the substrate [281]. The APSFET (adsorption porous silicon-based field effect transistor) concept developed by Barillaro and co-workers is interesting because in this design there is no need to fabricate electrodes after the formation of the PSi layer [282]. The APSFET has been used, for example, to detect ppb levels of NO_2 [283]. In addition, humidity sensing and detection of a variety of different organic species has been demonstrated with PSi-based

sensors [277].

Electrical sensors are usually based on monitoring the changes in capacitance or resistance. The adsorption of gases causes changes in the effective dielectric constant and the conductivity of the PSi layer. The APSFET sensor has a slightly differing operational principle, since it only measures the conductivity of the Si channel below the PSi layer [282]. In the conventional designs, where electrodes are patterned on top of the PSi surface, current may travel mainly through the Si substrate, instead of the PSi layer, due to the lower conductivity of PSi. This naturally lowers the sensitivity of the PSi sensor. However, the sensitivity may be considerably increased by electrically isolating the PSi layer from the substrate [232]. This can be achieved by fabricating an oxidized PSi layer beneath the sensing layer [232].

As a result of capillary condensation, described by the Kelvin equation (2.16), the adsorption and desorption kinetics for mesoporous materials differ from each other. This causes hysteresis, which is clearly observed in PSi based sensors. Fortunately, several methods for hysteresis reduction have been developed [284]. Increasing the average pore size by means of annealing is an effective method. Furthermore, the operating temperature of the sensor may also be increased with an integrated heater, in order to assist the out-diffusion of gases. However, both of these methods result in reduced sensitivity [284]. Moreover, surface chemistry also affects the hysteresis behaviour, mainly by increasing or decreasing the affinity of an adsorbate towards the surface [106].

2.7.2 Optical Sensing

In the early 1990s, Prof. Sailor's group discovered that the photoluminescence of PSi is quenched in the presence of vapors [285, 286]. This has enabled using the PL properties of PSi in sensing applications [83]. However, PSi-based passive optical elements are utilized in sensing applications more frequently than PL. In 1996, Bjorklund and co-workers reported on color changes in PSi thin films upon exposure to vapors of organic solvents [79]. An important finding was that the effective refractive index of the layer changes reversibly during the adsorption of vapors inside the porous layer [79]. They followed up on the research and used ellipsometry for detection of water, ethanol, and acetone vapors [287]. In 1999, Paul Snow et al. demonstrated that the change in the effective refractive index upon vapor adsorption translates into a redshift of the reflectance spec-

trum of a PSi-based interference filter [80]. Since then, similar structures, such as optical microcavities, have been used in different sensing applications [89, 93, 288, 289]. Recently, other approaches to optical sensing have been proposed, e.g., the utilization of PSi-based waveguides [91, 92, 290].

Optical detection systems have one distinct advantage over the electrical sensors, namely optical sensors enable remote reading. Moreover, no wiring, control electronics, or power source for sensors are necessary. An interesting application utilizing this aspect has been demonstrated by King and co-workers [291]. They attached free-standing PSi rugate filters to the tip of an optical fibre, and used it for monitoring vapor breakthrough in an activated carbon filtration cartridge used in respirators [291, 292]. Another interesting aspect of sensors based on PSi interference filters is the possibility to fabricate stacked structures with differing surface chemistries [293, 294]. These stacked filter structures have been used for removing the effect of humidity to achieve repeatable signals to analyte exposure under atmospheres with varying levels of humidity [294].

2.7.3 Multiparametric Sensing

Even though sensitive detection of several gases has been demonstrated with PSi-based electrical and optical sensors, selectivity, i.e., the ability to discriminate between adsorbing gases, is a problem that has mostly remained unanswered. It has been shown that surface chemistry has a distinct effect on the affinity of adsorbate molecules towards the PSi surface [292], and that differing surface chemistries can be utilized to rule out fluctuations in the atmospheric composition caused by, e.g., changes in humidity [294]. Internally referenced sensors can also be prepared by infiltrating polystyrene inside the PSi matrix [295], which is a simple method for increasing selectivity. Another approach for obtaining selectivity, is to use a surface termination that reacts with certain gases in an irreversible fashion. For example, monitoring the corrosion of as-anodized and oxidized PSi surfaces caused by HF or Cl_2 [295, 296] gases has been shown to be a feasible method for achieving highly selective single-use sensors. However, sensing schemes utilizing irreversible reactions are restricted to specific gases, and are thus difficult to generalize.

As we have discussed above, it is often difficult, if not impossible, to selectively detect a certain analyte vapor using only a single detection parameter. Multiparametric detection has been proposed as a simple method

for increasing the ability of a sensor to differentiate between a variety of vapors. In addition to sensitivity, this provides a way to rule out false positives, which increases the detection capability of the sensor. Results on the first multiparametric sensors based on PSi were published in 2000 [297, 298]. For instance, simultaneously monitoring thin film reflectance and PL enabled Létant et al. to discriminate among a large number of vapors, with the results being comparable to the performance of a commercial electronic nose [297]. The group of Lorenzo Pavesi has used PSi optical microcavities and by monitoring electrical current and PL, they showed that it is possible to differentiate between NO_2 and humidity [299]. The sensitivity was further improved by using an array type configuration [281]. A PSi-based sensor array, utilizing exclusively reflectance measurements, has also been demonstrated [300]. An interesting method, which has also been proven quite sensitive, is a technique where the color-difference of an image taken from the surface of PSi optical reflector is monitored upon vapor exposure [301]. By comparing the change in the color of individual pixels of the entire image, the authors were able to detect 140 ppm concentration of ethanol vapor [301].

Although many different multiparametric sensing systems have already been demonstrated, there are still a lot of possibilities for combining different sensing methods to increase the selectivity of sensor designs. The versatility of PSi enables the tailoring of many properties such as pore size and surface chemistry to accommodate different sensing scenarios. In addition, PSi can be used as a reductive template for metal salts, which can also be utilized in sensing. For example, Pd modified PSi has been used as a hydrogen sensor [302–304].

Chapter 3

Aims of the Study

In previous studies, thermal carbonization has been established as an effective method for stabilizing the reactive surface of PSi and also as a suitable surface treatment method for sensing applications. The main purpose of this study was to investigate the effectiveness and feasibility of the TC treatment in stabilizing PSi optical filters for sensing applications. In addition to studying the effects of the TC treatment on the optical properties of PSi, a secondary objective was to confirm if the favourable electrical properties of TCPSi, namely increased electrical conductivity, could be used to produce a stable multiparametric sensor.

In effort to finding answers to the unresolved questions presented above, new ones were created. Some of these new questions were also actively pursued. First of all, the effects of more complicated filter structures to the gas sensing properties were explored, in detail. The purpose was to find all-optical methods for increasing selectivity in PSi-based gas sensors. To that end, methods for preparing rugate filters displaying multiple stopbands were studied. Another motivating factor for that particular study was the desire to determine what kind of an effect would sidelobe suppression methods have on the adsorption and desorption behaviour of gases into mesoporous Si rugate filters, and secondly whether or not it would be possible to improve spectral quality without compromising sensitivity.

The final aim of the study was to conduct a detailed comparison on the differences in stability and sensitivity of various chemically modified PSi optical filters under amine exposure. The main intention was to exploit the exceptional stability of carbonized PSi and try to create stable optical filters with a functional group attached to the surface. In this case, undecylenic acid functionalization was used and a comparison between as-anodized and thermally hydrocarbonized porous silicon was conducted. Stable and func-

tionalized PSi surfaces are of great interest for developing reliable biosensors, and the carboxyl group in undecylenic acid enables further biofunctionalization of the surface for different applications.

Chapter 4

Experimental

4.1 Reflectance Spectroscopy

Measuring the reflection of light from a specimen is a simple method which can be used to gather information regarding the properties of the sample. The most general definition for reflectance ρ is as the ratio of the reflected and incident radiant fluxes, Φ_r and Φ_i [305]:

$$\rho = \frac{\Phi_r}{\Phi_i}. \tag{4.1}$$

Spectral reflectance for a specified wavelength λ is similarly defined as:

$$\rho(\lambda) = \frac{\Phi_{\lambda r}}{\Phi_{\lambda i}}. \tag{4.2}$$

In actual experiments, the spectral reflectance factor R is usually measured, which is the ratio of spectral flux reflected from a sample to the spectral flux which would be reflected by a perfect diffuse (lambertian) reflector [305]. This measurement can be done with a light source, a detector, and an optical fibre.

In papers I, II, and III reflectance spectra were measured with a simple photodetector and the wavelength of light was controlled with a monochromator. In papers IV and V a spectrophotometer (Ocean Optics, HR4000CG-UV-NIR) was used for recording the reflectance spectra. The measurements in the first three papers were mainly conducted in the infrared region and a xenon short arc lamp was used as a light source. In the last two papers, visible range measurements were made with a tungsten halogen lamp.

4.2 Fourier Transform Infrared Spectroscopy

Fourier Transform Infrared Spectroscopy (FTIR) is a dynamic instrumental technique that can be applied to an enormous variety of samples. The FTIR method is based on absorption of infrared radiation by a chemical bond when the resonant frequency of the bond equals the frequency of the incident radiation. Chemical bonds may have several vibrational modes and the FTIR enables qualitative and quantitative analysis for specimen in gas, liquid, or solid phase. The interaction between the infrared radiation and the sample, in the form of absorbance A, is described by the Beer-Lambert law, which relates the infrared band intensity to concentration:

$$A = \log_{10} \frac{1}{T} = -\log_{10} T = \epsilon l c, \tag{4.3}$$

where T is transmittance, ϵ is the absorptivity, l is the path length, and c is the concentration of the sample [306]. Deviations from the linear relationship can be caused by the effect of stray radiation, insufficient resolution, and chemical effects. The principal factor leading to deviations from Beer-Lambert law in FTIR spectrometers is the effect of insufficient resolution [306].

FTIR measurements were used throughout this thesis for determining vapor concentrations by using the ideal gas law. Measurements were done with a Spectrum BX (Perkin Elmer) FTIR spectrometer in papers I-III, and with a FT/IR-460 Plus (Jasco) spectrometer in papers IV and V. In addition, the chemical composition of thermally oxidized PSi was confirmed with FTIR measurements in paper IV.

4.3 Nitrogen Sorption

Nitrogen adsorption at a temperature of -196°C can be used for determining surface area and pore size distribution of a mesoporous material [307]. The determinations are based on the BET (Brunnauer-Emmett-Teller) and BJH (Barret-Joyner-Halenda) theories [145, 308], which enable the determination of surface area and pore size distribution from sorption isotherms measured with the nitrogen sorption apparatus. Usually the desorption branch of the isotherm is preferred when determining pore size distribution.

Nitrogen sorption measurements were used in paper III for determining the surface area and pore size distributions for different samples. The measurements were done with the TriStar 3000 (Micromeritics).

4.4 Scanning Electron Microscopy

The scanning electron microscope (SEM) is a commonly used instrument which enables the observation of organic and inorganic materials on a nanometer to micrometer scale. In addition to high spatial resolution, the SEM provides a depth of field large enough for obtaining three-dimensional-like images. For these reasons the SEM is an invaluable tool for obtaining information about surface topography. The working principle of the SEM is based on the detection of signals that result from scanning the sample with a high-energy beam of electrons. An electron gun is used to create the electron beam which is then focused with electron lenses. Scan coils are used for sweeping the beam across the surface of a sample in a raster-pattern. An electron detector, such as the Everhart-Thornley detector [309], is used for obtaining a signal from secondary electrons and/or backscattered electrons. This signal is used for creating an image of the sample. Other type of signals such as characteristic X-rays may also be recorded with appropriate detectors. A detailed description regarding the principles and operation of the SEM can be found, for example, from a book written by Goldstein et al. [310].

In this work, scanning electron microscopy was used in papers IV and V for obtaining cross-sectional micrographs of PSi optical filters. The measurements were done for carefully cleaved samples by using a JEOL JSM-6500FE or a Carl Zeiss STM Ultra 55 FE-SEM for secondary electron imaging. The images gave information regarding the depth of the porous layers. Additionally, sample quality could also be roughly assessed by inspecting the homogeneity of the porous layers.

4.5 X-Ray Photoelectron Spectroscopy

In X-ray photoelectron spectroscopy (XPS), low-energy electrons are liberated from the sample as a result of the photoemission process [311, 312]. An electron spectrometer consists of a source of primary radiation (soft X-rays), and an electron energy analyzer, both contained within a vacuum

chamber. Electrons ejected from a core level, by an X-ray photon of energy $h\nu$, are observed. The experimental quantity measured by the spectrometer is the kinetic energy, E_{K}. The binding energies, E_{B}, of ejected electrons are related to the kinetic energy as follows:

$$E_{\mathrm{B}} = h\nu - E_{\mathrm{K}} - W, \tag{4.4}$$

where W is the spectrometer work function [311]. Since all the parameters on the right-hand side are known, we can determine the binding energies for ejected electrons.

XPS measurements were used in paper V for monitoring the changes in chemical composition and chemical binding states of the PSi samples as they were exposed to highly oxidizing amine vapors. A JEOL JPS-9010MC X-ray photoelectron spectrometer was used with an Al K_α line as the X-ray source.

4.6 Other Methods

Gas-liquid chromatography (GLC) was used for determining methyl- and trimethylamine vapor concentrations in paper V. CLG analysis was performed on a Shimadzu GC-14B instrument equipped with a flame ionization detector and a CP-Volamine capillary column (Agilent, 30 m $\times$ 0.32 mm).

Chapter 5

Results and Discussion on Papers

In the following chapter, a summary of the most important results gathered from the original papers is presented. Some unpublished data is also included. The purpose of this chapter is to present the core results of the thesis in a clear and concise manner.

5.1 Paper I

In paper I, the use of thermal carbonization (TC) as a method for stabilizing porous silicon optical filters was studied. In comparison to many oxidation treatments, which have been applied to passivation of PSi-based optical filters in the past, the TC treatment does not lead to a large decrease in the specific surface area of PSi. Therefore, TC is a promising method for stabilizing PSi structures for sensing applications. In this study, TC was found to decrease the optical refractive index of porous silicon (Fig. 5.1). As a result, the shape of the reflectance spectrum measured for carbonized Bragg reflectors was slightly changed, but the changes were quite negligible.

Long-term stability was evaluated by storing the samples in ethanol for a period of six months. The resulting changes in the reflective peak position were evaluated periodically by measuring the reflectance spectra. Changes in the peak position as a function of storage time are presented in Fig. 5.2. For the as-anodized sample, a clear blueshift is observed which indicates that the sample is heavily oxidized. The changes measured for the carbonized and the hydrocarbonized sample were small. Fluctuation in the peak position, are attributed to changes in the measurement position of

the spectrum on the sample surface. These experiments confirm that both carbonization treatments protect the PSi filters against oxidation thus preserving the optical performance and enabling long-term sensing scenarios. Some preliminary results on sensing vapors of organic compounds were also reported, which showed that the gas sensing properties of carbonized PSi are different from as-anodized PSi.

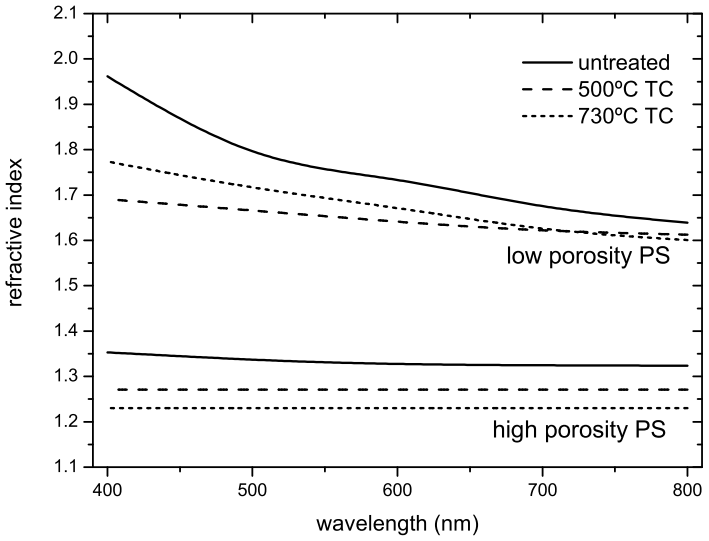

Figure 5.1: Porous silicon refractive index determined for as-anodized and thermally carbonized porous silicon thin films prepared with $10\,\mathrm{mA/cm^2}$ and $150\,\mathrm{mA/cm^2}$ anodization currents densities.

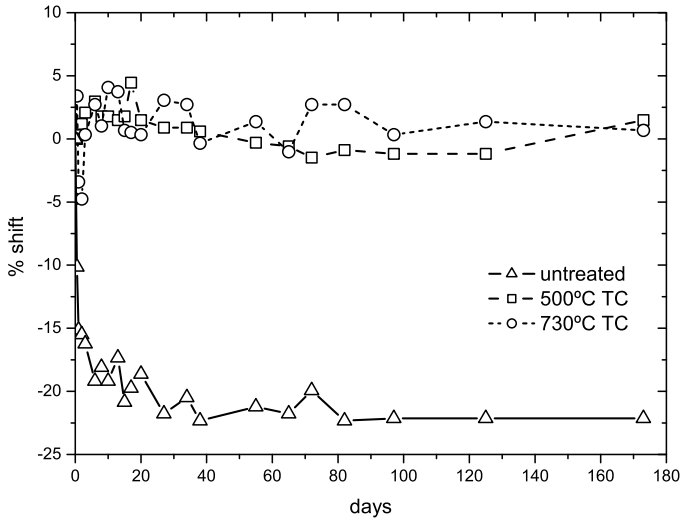

Figure 5.2: Relative change of the reflective peak position presented as a function of storage time in ethanol. The as-anodized sample shows a prominent blueshift, which indicates that the effective refractive index of the porous structure is decreased as a result of oxidation. The carbonized reflectors display only slight fluctuatuation, which is mostly due to differences in the measurement spot on sample surface.

5.2 Paper II

Following up on the results presented in paper I, paper II focuses on analysing the gas sensing properties of hydrocarbonized Bragg reflectors in detail. This was done by studying the adsorption and desorption behaviour of six organic compounds.

All studied gases produced a clear redshift of the reflectance spectrum. An example of this can be seen from the reflectance spectra measured under increasing concentrations of hexane (Fig. 5.3). The redshift increased linearly as a function of gas concentration for most studied gases. However, hexane vapor displayed non-linear behaviour (Fig. 5.4). This might be related to capillary condensation, which depends on the saturated va-

por pressure of the studied gas, the pore size distribution of the PSi-based reflector, and chemical properties of the surface.

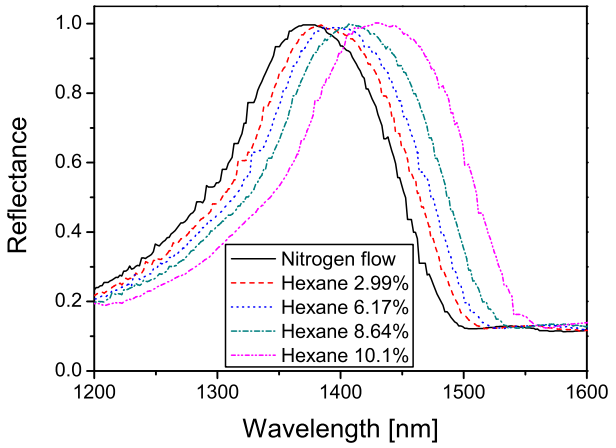

Figure 5.3: Reflectance spectra measured for a thermally hydrocarbonized PSi Bragg reflector, when exposed to varying concentrations of hexane vapor.

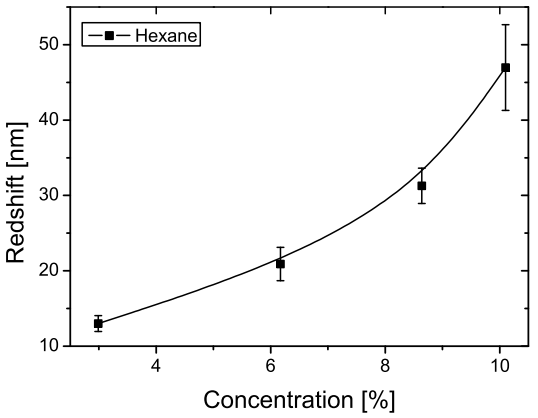

Figure 5.4: Redshift values, measured under hexane vapor exposure, exhibit non-linear behaviour as a function of vapor concentration.

In addition to the observed redshift, it was discovered that vapor ex-

posure also resulted in changes in the shape of the reflectance spectrum. The changes were analyzed by measuring the full width at half maximum (FWHM) values of the stopband. Exposure to acetone vapor resulted in a clear increase in the observed FWHM value. The increase was obvious even after the FWHM values were normalized to rule out the stopband-widening effect related to the redshift. In contrast, a decrease in the width of the stopband was observed in the case of methylamine and decane. We also demonstrated that this phenomenon can be used to differentiate between vapors that produce equally large redshifts, by comparing the redshift and FWHM values measured for different concentrations of acetone and methylamine vapors.

Finally, time-resolved measurements were performed in order to study sorption kinetics of the studied vapors. Measurements were conducted by setting the detection wavelength to a fixed value that corresponded to a spectral position on the right-hand side of the steep slope of the stopband. As a consequence, the adsorption-induced redshift resulted in an increase in reflected light intensity. An example for acetone vapor is shown in Fig. 5.5. The response times for the studied vapors were fast, with slight variations among different compounds. Also, the signal did not display baseline drift indicating that the reflectors were chemically stable.

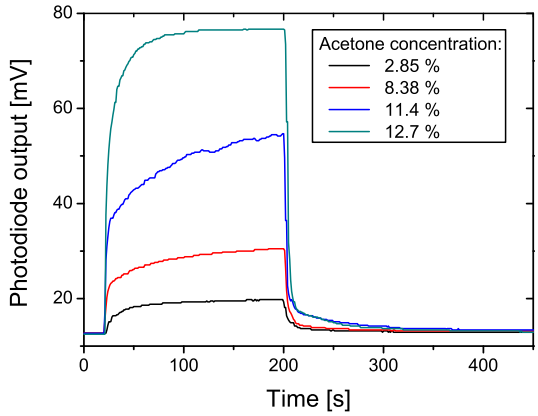

Figure 5.5: Photodiode output voltage at $\lambda = 1520\,\text{nm}$ as a function of time. Rapid response to acetone vapor is observed at $t = 20\,\text{s}$, when acetone is introduced to the sensing chamber. Recovery from acetone exposure under nitrogen flow is also fast.

5.3 Paper III

In paper III, the possibility for using both electrical and optical signals from a THCPSi and a TCPSi sensor to increase the sensors ability to differentiate among different gases was explored. In previous studies, the electrical properties of TCPSi have been found favourable for preparing capacitive humidity and gas sensors [230–232, 313]. We also wanted to know if the electrical detection would have an effect on the optical signal from a PSi interference filter.

The practical implementation was carried out by preparing large-area rugate layers, which were thermally carbonized at 500 °C or 700 °C. Gold electrodes were sputtered on the top surface and copper wires were attached to the electrodes to enable acquisition of an electrical signal from the porous layer. The carbonization and hydrocarbonization treatments not only resulted in differences by imparting hydrophobic or hydrophilic character to the surface, but also, a change in the pore diameter and specific surface area was observed. The differences are illustrated in Figure 5.6, where the pore size distributions, calculated with the BJH method from nitrogen desorption curves, are shown for two free-standing films treated with the hydrocarbonization and carbonization treatments.

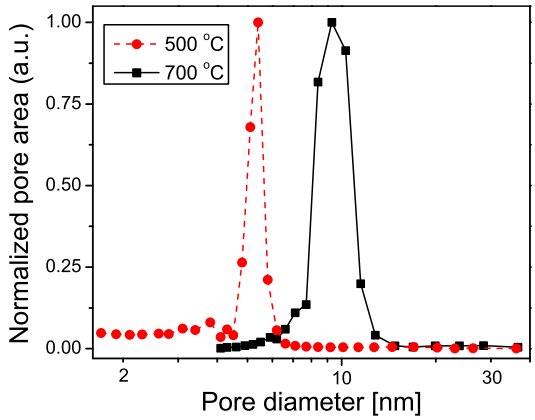

Figure 5.6: Pore size distribution determined for free-standing PSi membranes produced with anodization current density of 10 mA/cm^2. Thermal carbonization at 700 °C enlarges the pores in comparison to treatment at 500 °C.

Proof of concept was showed by demonstrating that both the hydrophilic sensor (treated at 700 °C) and the hydrophobic sensor (treated at 500 °C) allowed the simultaneous detection of capacitance and reflectance, producing characteristic traces when subjected to varying amounts of dimethylformamide, ethanol, and relative humidity. The hydrophobic sensor did not produce a signal large and clear enough for detection of humidity changes, which was expected. The hydrophilic sensor gave clearly distinguishable signals for all three vapors. The electro-optical response as a function of relative pressure is shown in Fig.5.7, for both sensor types.

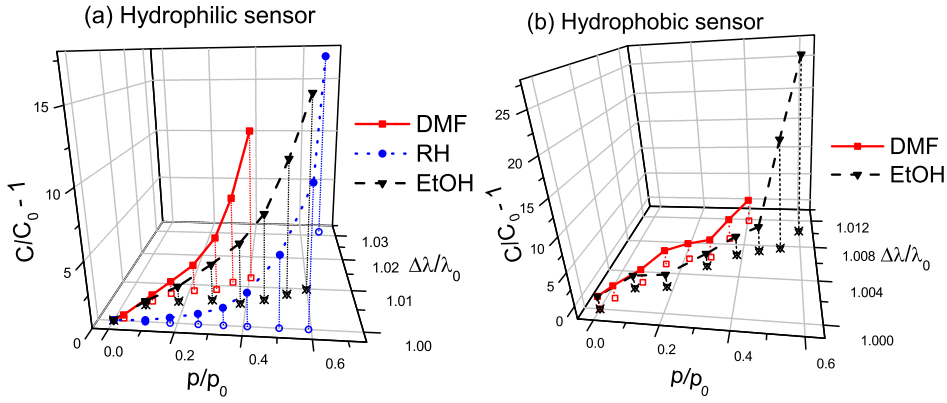

Figure 5.7: Optical and electrical response curves determined as a function of relative vapor pressure for the hydrophilic (a) and hydrophobic (b) sensor. The three-dimensional migration curves for dimethylformamide and ethanol are distinctive, thus enabling differentiation between the two adsorbates. In addition, an original trace related to an increase in relative humidity can be produced with the hydrophilic sensor.

With regards to sensitivity, our studies revealed that the optical performance of the rugate filter was not affected by the addition of gold electrodes on the surface. This was expected, since the electrodes only occupy a small area of the total surface, and because the optical measurement takes place in a position that is slightly removed from the electrodes. However, the electrical performance, i.e. the capacitive response, was far from optimal. This was observed when the results were compared to an optimized TCPSi capacitive-type humidity sensor [232]. The lowered electrical performance is probably related to the porosity modulation of the rugate filter. It is

well-known that the resistance of a PSi layer increases as a function of porosity, so this phenomenon undoubtedly has an effect on the electrical sensing characteristics.

5.4 Paper IV

The purpose of paper IV was to thoroughly examine the preparation of rugate filters that display multiple stopbands. In particular, focus was placed on investigating the effects that structural differences have on gas adsorption. Sidelobe suppression methods for improving spectral quality were also employed, and the observed effects, relevant to gas sensing applications, were demonstrated. One of the motivating factors for this study was to explore fully optical methods for increasing differentiation capabilities of the PSi sensor elements. This approach was chosen due to the observations presented in paper III, where the capacitive-signal for the electro-optical sensor displayed lowered sensitivity in comparison to a purely electrical sensor.

Preparation of dual-peak filters was accomplished by placing two sinusoidal anodization current profiles in series or in superposition. We confirmed that both methods resulted in structures displaying reflectance peaks at indentical wavelengths. However, when placing optical filters in series, the order in which the single-line filters were stacked on top of each other proved out to be extremely important. We noticed that single-line filters displaying a peak in a wavelength region that exhibits high optical absorption should be placed on top in order to insure the appearance of the corresponding peak in the reflectance spectrum. In the superimposed filter structure, this limitation does not obviously exist. Another difference between the two preparation methods was the appearance of interference fringes on top of stopbands originating from lower filter layers in the stacked filter-configuration. This phenomenon was attributed to the interfaces between the individual filter layers, and the resulting interference effects. Figure 5.8 presents a cross-sectional SEM micrograph of two stacked rugate filters, with the interface between the filters clearly visible.

Interference fringes, also referred to as sidelobes, result from interference of light between the air-PSi and the PSi-substrate interfaces. An additional interface is formed when two single-line filters are prepared on top of each other. The effectiveness of refractive index matching as a method for side-

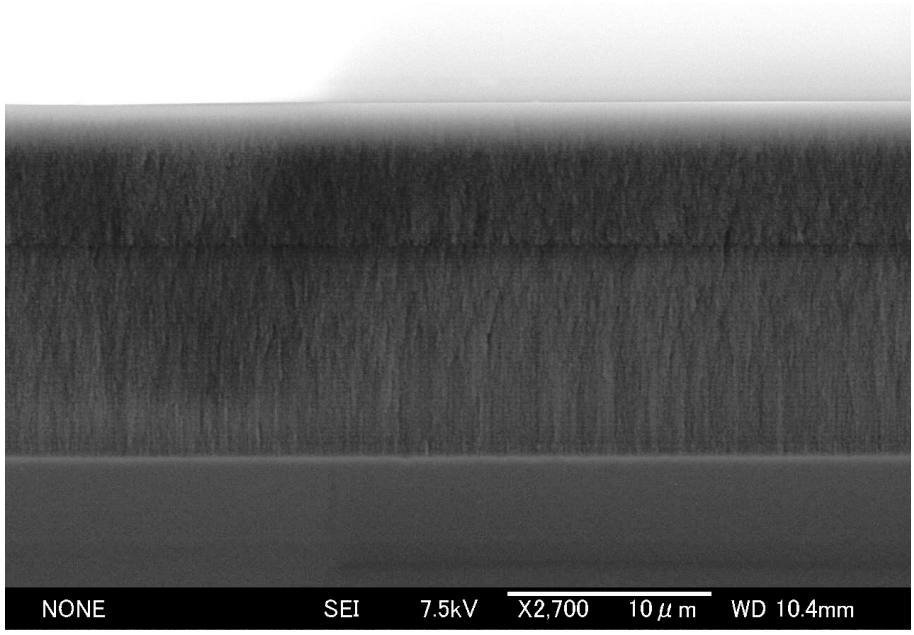

Figure 5.8: Cross-sectional SEM micrograph of stacked porous silicon rugate filters prepared on a silicon substrate. The filter on top displays a reflectance peak around 500 nm. The interface between the layers causes interference effects, which result in the appearance of fringes in the reflectance spectrum on the reflectance peak originating from the lower layer.

lobe suppression was examined for multipeak filters. Figure 5.9 displays the effect of index mathing layers on the reflectance spectrum of a dual-peak rugate filter composed by stacking two single-line filters. The addition of index matching layers has a pronounced effect on the intensity of the sidelobes, and the interference fringes on top of the second reflective peak are also greatly reduced. Gaussian apodization was also studied for reducing sidelobe intensity (Fig. 5.10). Based on our observations, Gaussian apodization was not effective in suppressing the sidelobes in a wavelength region where optical absorption and dispersion were prominent.

Sensitivity and recovery for different filter configurations proved to be variant under ethanol exposure. The superimposed structures exhibited faster recovery, which was attributed to a smaller overall thickness of the

porous filter. On the other hand, the stacked structures were slightly more sensitive. The sensitivity can be explained by the slightly smaller pore diameters. The addition of refractive index matching layers in order to reduce sidelobes did not have an adverse effect on the sensing capabilities of the studied filter structures. Therefore, it proved to be an effective method for improving spectral quality of stacked multipeak filters without compromising the performance of the sensor.

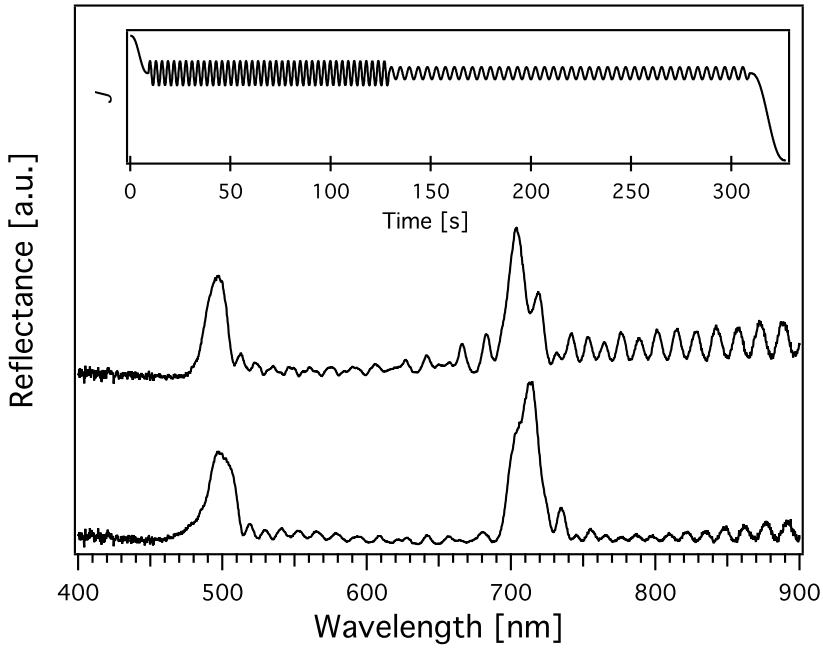

Figure 5.9: Effect of quintic refractive index matching layers for a stacked filter design is demonstrated by preparing otherwise identical dual-peak filters, with (lower spectrum) and without (upper spectrum) matching layers. The inset displays the anodization current density profile with quintic refractive index mathing included. The addition of index matching layers visibly improves the spectral quality of the second stopband located around 700 nm.

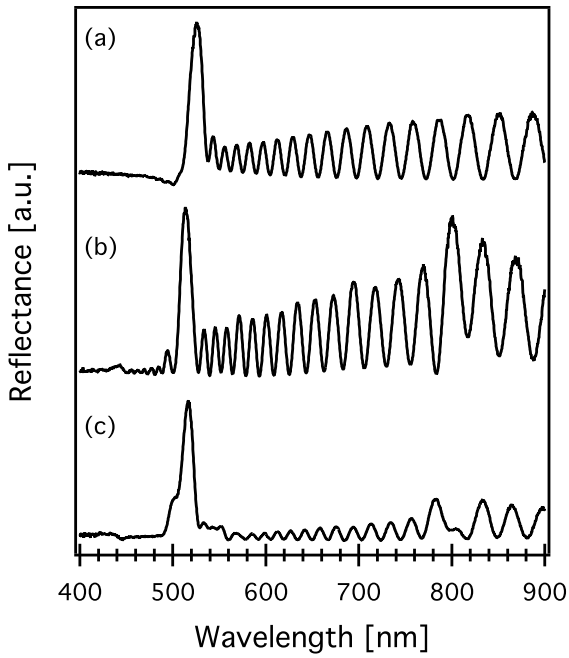

Figure 5.10: Effects of Gaussian apodization in a wavelength region where optical absorption and dispersion are not negligible. Rugate filters produced with anodization current profiles corresponding to a sinusoidal current (a), sinusoidal current with Gaussian apodization (b), and sinusoidal current with Gaussian apodization and quintic refractive index matching (c).

5.5 Paper V

Paper V concentrated on finding the differences in stability and sensitivity of PSi optical microcavities with different surface modifications, when subjected to highly oxidizing methyl- and trimethylamine vapors. Also, the possibility of forming a microcavity between two rugate filters was investigated. In addition to reflectance measurements, X-ray photoelectron spectroscopy (XPS) was used in assessing the degree of oxidation after the sensing experiments.

Along with the TC and THC treatments, thermal hydrosilylation of un-

decylenic acid with PSi (UnPSi) and undecylenic acid functionalized THC (UnTHC) were also studied as potential methods for chemically passivating the PSi surface. Successful carboxylic acid functionalization of the UnPSi and UnTHC microcavities was confirmed with XPS (Fig. 5.11). The effect of the UnPSi and UnTHC treatments to the reflectance spectra of PSi optical microcavities was also studied (Fig. 5.12). A redshift was observed for both treatments which corresponds to undecylenic acid binding on the inner surface of PSi. Moreover, for UnTHCPSi, an initial blueshift related to the hydrocarbonization treatment was observed, which was followed by a successive and slightly larger redshift as the THCPSi was functionalized with undecylenic acid.

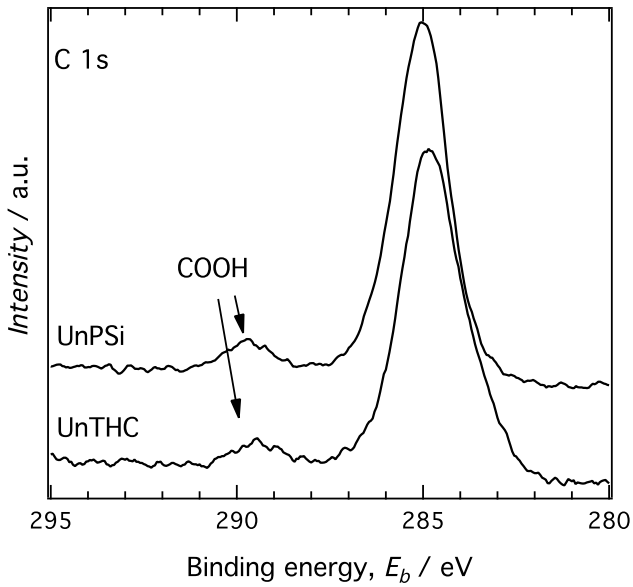

Figure 5.11: C 1s core level spectra for UnPSi and UnTHCPSi optical microcavities. The small feature at 289.5 eV is assigned to the carboxylic functional group.

The surface chemistry had a large effect on the sensitivity of the PSi optical microcavities towards methylamine, trimethylamine, and ethanol vapors. Moreover, the highly oxidizing amine vapor environment had a detrimental effect on the stability of the UnPSi microcavities, and large

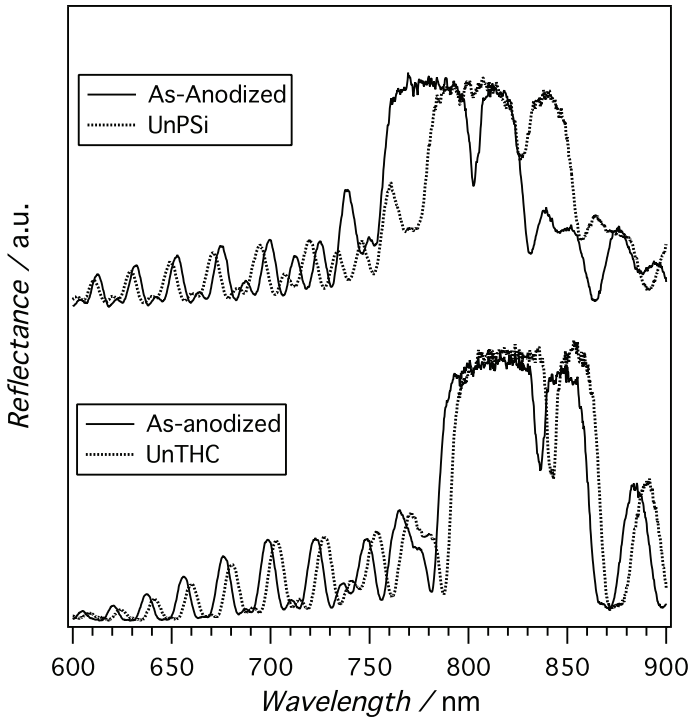

Figure 5.12: Reflectance spectra for two PSi optical microcavities before (solid line) and after (dotted line) UnPSi (upper traces) and UnTHC (lower traces) treatments.

baseline drift was observed in the reflectance spectra. Additionally, XPS measurements revealed that the UnPSi samples were heavily oxidized. On the other hand, TC, THC, and UnTHC surface modifications resulted in greater stability and only minor changes in the reflectance and XPS spectra could be observed after the sensing experiments. The reflectance spectra for THC and UnTHC microcavities did not show discernible baseline drift, whereas the TC microcavity spectra displayed a small irreversible redshift, which was attributed to surface oxidation. This conclusion was supported by a growth in the oxide related peaks in XPS core level spectra measured for TCPSi.

The TC modified cavities had the largest sensitivity towards all the studied vapors. However, the growth of an oxide layer on the inner surface

of the TCPSi samples during sensing experiments had an effect on the measured redshift value. A plausible explanation for this observation is that capillary condensation is more easily promoted as the pores become slightly narrower due to the oxide layer formation inside the pores. The UnTHC modified cavities showed larger sensitivity towards amines in comparison to the THC modified microcavities. Conversely, UnTHC response to ethanol vapor was the smallest. Average redshifts measured under methylamine exposure for the three surface chemistries are shown in Fig. 5.13.

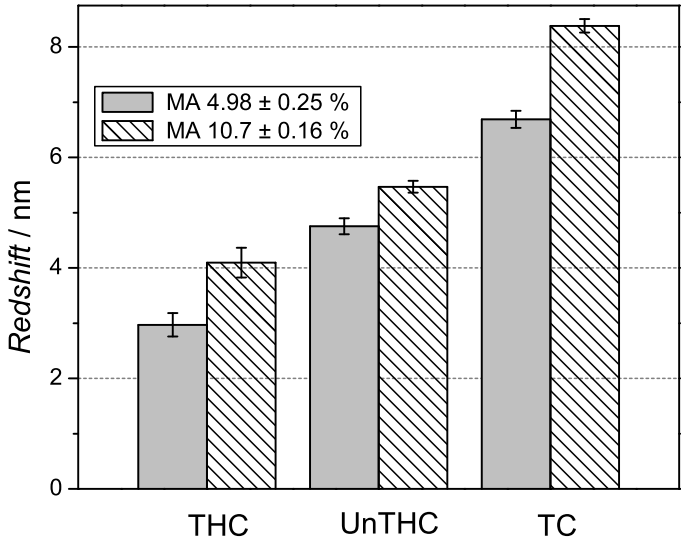

Figure 5.13: Average redshifts measured for THC, UnTHC, and TC treated PSi optical microcavities when exposed to methylamine. Methylamine concentration is indicated as volumetric fraction.

Chapter 6

Conclusions

In the present study, thermal carbonization was established as a feasible method for stabilizing PSi optical filters. In addition, the gas sensing properties of carbonized PSi-based filters were found favorable for reliable long-term sensing applications. We also observed an interesting behaviour related to the effects of gas adsorption, namely changes in the FWHM value of the stopband. It was shown that this phenomenon may be used to distinguish one adsorbate from another. Another method for increasing the selectivity of carbonized PSi-sensors was using capacitive sensing simultaneously while monitoring changes in the optical properties. Multiparametric sensing did not have discernible effects on the optical gas sensing properties, but the capacitive sensitivity was clearly reduced. Nevertheless, this method allowed for simple detection with greatly increased abilities for differentiating among several gases.

No attempt was made at optimizing the structure of the multiparametric sensor for improving the capacitive sensing properties. Also, the response of the sensor for gas mixtures was not tested. Therefore, the differentiation capabilities of the sensor under atmospheres that would be more realistic for many practical applications remain uncharted. These are important questions that should be pursued in further studies.

The use of multistopband rugate filters in gas sensing was also studied. Both stacked and superimposed structures were investigated and small differences in respective gas sorption kinetics were found. Moreover, quintic refractive index matching layers were found effective in suppressing sidelobes without having an adverse effect on the sensing properties. For future studies, the use of different carbonization treatments, namely TC and THC, in multipeak rugate filters offers new possibilities and we have already been able to produce some promising results [314].

Both TC and THC treatment were observed to preserve the optical properties of PSi-based filters under highly oxidizing atmospheric conditions with high amine concentration. More importantly, similar stability was observed when the THC surface was functionalized with undecylenic acid. The difference in stability compared to a sample with conventional undecylenic acid functionalization was significant. Stable PSi-based optical filters with a functional surface are important for label-free biosensing applications. The results presented in this thesis suggest that more research regarding the use of the UnTHC surface in this context should be conducted.

Bibliography

[1] A. Uhlir, Bell Labs Tech. J. **35**, 333 (1956).

[2] A. Uhlir and I. Uhlir, Phys. Status Solidi C **2**, 3185 (2005).

[3] D. R. Turner, J. Electrochem. Soc. **105**, 402 (1958).

[4] R. J. Archer, J. Phys. Chem. Solids **14**, 104 (1960).

[5] R. Memming and G. Schwandt, Surf. Sci. **4**, 109 (1966).

[6] Y. Watanabe and T. Sakai, Rev. Electron. Commun. Labs. **19**, 899 (1971).

[7] M. J. J. Theunissen, J. A. Appels, and W. H. C. G. Verkuylen, J. Electrochem. Soc. **117**, 959 (1970).

[8] M. J. J. Theunissen, J. Electrochem. Soc. **119**, 351 (1972).

[9] Y. Watanabe, Y. Arita, T. Yokoyama, and Y. Igarashi, J. Electrochem. Soc. **122**, 1351 (1975).

[10] Y. Arita and Y. Sunohara, J. Electrochem. Soc. **124**, 285 (1977).

[11] Y. Arita, J. Cryst. Growth **45**, 383 (1978).

[12] T. Unagami, Jpn. J. Appl. Phys. **19**, 231 (1980).

[13] T. Unagami, J. Electrochem. Soc. **127**, 476 (1980).

[14] K. Imai, Solid State Electron. **24**, 159 (1981).

[15] S. Konaka, M. Tabe, and T. Sakai, Appl. Phys. Lett. **41**, 86 (1982).

[16] R. P. Holmstrom and J. Y. Chi, Appl. Phys. Lett. **42**, 386 (1983).

[17] K. Imai and H. Unno, IEEE T. Electron Dev. **31**, 297 (1984).

[18] G. Bomchil, A. Halimaoui, and R. Herino, Appl. Surf. Sci. **41/42**, 604 (1989).

[19] T. Yonehara, K. Sakaguchi, and N. Sato, Appl. Phys. Lett. **64**, 2108 (1994).

[20] K. Sakaguchi, N. Sato, K. Yamagata, T. Atoji, Y. Fujiyama, J. Nakayama, and T. Yonehara, IEICE T. Electron. **E80**, 378 (1997).

[21] C. Pickering, M. I. J. Beale, D. J. Robbins, P. J. Pearson, and R. Greef, J. Phys. C Solid State **17**, 6535 (1984).

[22] L. Canham, Appl. Phys. Lett. **57**, 1046 (1990).

[23] V. Lehmann and U. Gösele, Appl. Phys. Lett. **58**, 856 (1991).

[24] U. Gösele and H. Föll, ECS Transactions **16**, 7 (2008).

[25] A. Richter, P. Steiner, F. Kozlowski, and W. Lang, IEEE Electr. Device L. **12**, 691 (1991).

[26] A. Halimaoui, C. Oules, G. Bomchil, A. Bsiesy, F. Gaspard, R. Herino, M. Ligeon, and F. Muller, Appl. Phys. Lett. **59**, 304 (1991).

[27] N. Koshida and H. Koyama, Appl. Phys. Lett. **60**, 347 (1992).

[28] A. G. Cullis and L. Canham, Nature **353**, 335 (1991).

[29] A. Bsiesy, F. Muller, M. Ligeon, F. Gaspard, R. Herino, R. Romenstain, and J. C. Vial, Phys. Rev. Lett. **71**, 637 (1993).

[30] L. Canham, Nature **365**, 695 (1993).

[31] F. Muller, R. Herino, M. Ligeon, F. Gaspard, R. Romenstain, J. C. Vial, and A. Bsiesy, J. Lumin. **57**, 283 (1993).

[32] L. T. Canham, *Properties of Porous Silicon* (INSPEC, London, United Kingdom, 1997), chap. Visible photoluminescence from porous silicon, pp. 249–255.

[33] P. M. Fauchet, L. Tsybeskov, C. Peng, S. P. Duttagupta, J. von Behren, Y. Kostoulas, J. M. V. Vandyshev, and K. D. Hirschman, IEEE J. Sel. Top. Quant. **1**, 1126 (1995).

[34] A. G. Cullis, L. T. Canham, and P. D. J. Calcott, J. Appl. Phys. **82**, 909 (1997).

[35] T. I. Cox, *Properties of Porous Silicon* (INSPEC, London, United Kingdom, 1997), chap. Electroluminescence from porous silicon using solid state contacts, pp. 290–310.

[36] G. Vincent, Appl. Phys. Lett. **64**, 2367 (1994).

[37] M. G. Berger, C. Dieker, M. Thönissen, L. Vescan, H. Lüth, H. Münder, W. Theiß, M. Wernke, and P. Grosse, J. Phys. D. Appl. Phys. **27**, 1333 (1994).

[38] V. Pellegrini, A. Tredicucci, C. Mazzoleni, and L. Pavesi, Phys. Rev. B **52**, 14328 (1995).

[39] M. G. Berger, R. Arens-Fischer, M. Thönissen, M. Krüger, S. Billat, H. Lüth, S. Hilbrich, W. Theiß, and P. Grosse, Thin Solid Films **297**, 237 (1997).

[40] U. Grüning, V. Lehmann, and C. M. Engelhardt, Appl. Phys. Lett. **66**, 3254 (1995).

[41] F. Müller, A. Birner, U. Gösele, V. Lehmann, S. Ottow, and H. Föll, J. Porous Mat. **7**, 201 (2000).

[42] A. Birner, R. B. Wehrspohn, U. Gösele, and K. Busch, Adv. Mater. **13**, 377 (2001).

[43] S. Matthias, F. Müller, C. Jamois, R. B. Wehrspohn, and U. Gösele, Adv. Mater. **16**, 2166 (2004).

[44] T. Trifonov, A. Rodríguez, L. F. Marsal, J. Pallarès, and R. Alcubilla, Sensor. Actuat. A **141**, 662 (2008).

[45] L. C. Parsons and G. T. Andrews, Appl. Phys. Lett. **95**, 241909 (2009).

[46] G. N. Aliev, B. Goller, D. Kovalev, and P. A. Snow, Appl. Phys. Lett. **96**, 124101 (2010).

[47] L. Thomas, G. N. Aliev, and P. A. Snow, Appl. Phys. Lett. **97**, 173503 (2010).

[48] M. Krüger, M. Marso, M. G. Berger, M. Thönissen, S. Billat, R. Loo, W. Reetz, H. Lüth, S. Hilbrich, R. Arens-Fischer, et al., Thin Solid Films **297**, 241 (1997).

[49] V. Torres-Costa, R. Martín-Palma, and J. M. Martínez-Duart, Mater. Sci. Eng. C **27**, 954 (2007).

[50] V. Torres-Costa and R. J. Martín-Palma, J. Mater. Sci. **45**, 2823 (2010).

[51] M. E. Kompan, J. Salonen, and I. Y. Shabanov, J. Exp. Theor. Phys. **90**, 324 (2000).

[52] D. Kovalev, G. Polisski, J. Diener, H. Heckler, N. Künzner, V. Yu. Timoshenko, and F. Koch, Appl. Phys. Lett. **78**, 916 (2001).

[53] J. Diener, N. Künzner, D. Kovalev, E. Gross, V. Yu. Timoshenko, G. Polisski, and F. Koch, Appl. Phys. Lett. **78**, 3887 (2001).

[54] L. T. Canham, Adv. Mater. **7**, 1033 (1995).

[55] J. Salonen and V.-P. Lehto, Chem. Eng. J. **137**, 162 (2008).

[56] S. C. Bayliss, L. D. Buckberry, I. Fletcher, and M. J. Tobin, Sensor. Actuat. A **74**, 139 (1999).

[57] S. C. Bayliss, L. D. Buckberry, P. J. Harris, and M. Tobin, J. Porous Mat. **7**, 191 (2000).

[58] A. V. Sapelkin, S. C. Bayliss, B. Unal, and A. Charalambou, Biomaterials **27**, 842 (2006).

[59] A. B. Foraker, R. J. Walczak, M. H. Cohen, T. A. Boiarski, C. F. Grove, and P. W. Swaan, Pharm. Res. **20**, 110 (2003).

[60] E. J. Anglin, L. Cheng, W. R. Freeman, and M. J. Sailor, Adv. Drug Deliver. Rev. **60**, 1266 (2008).

[61] J. Salonen, A. M. Kaukonen, J. Hirvonen, and V.-P. Lehto, J. Pharm. Sci. **97**, 632 (2008).

[62] V. S.-Y. Lin, K. Motesharei, K.-P. S. Dancil, M. J. Sailor, and M. R. Ghadiri, Science **278**, 840 (1997).

[63] A. Janshoff, K.-P. S. Dancil, C. Steinem, D. P. Greiner, V. S.-Y. Lin, C. Gurtner, K. Motesharei, M. J. Sailor, and M. R. Ghadiri, J. Am. Chem. Soc. **120**, 12108 (1998).

[64] A. Jane, R. Dronov, A. Hodges, and N. H. Voelcker, Trends Biotechnol. **27**, 230 (2009).

[65] F. Cunin, T. A. Schmedake, J. R. Link, Y. Y. Li, J. Koh, S. N. Bhatia, and M. J. Sailor, Nat. Mater. **1**, 39 (2002).

[66] J. L. Coffer, M. A. Whitehead, D. K. Nagesha, P. Mukherjee, G. Akkaraju, M. Totolici, R. S. Saffie, and L. T. Canham, Phys. Status Solidi A **202**, 1451 (2005).

[67] K. G. Jung, J. W. Schultze, M. Thönissen, and H. Münder, Thin Solid Films **255**, 317 (1995).

[68] Y. Y. Li, F. Cunin, J. R. Link, T. Gao, R. E. Betts, S. H. Reiver, V. Chin, S. N. Bhatia, and M. J. Sailor, Science **299**, 2045 (2003).

[69] I. Coulthard, D.-T. Jiang, J. W. Lorimer, T. K. Sham, and X.-H. Feng, Langmuir **9**, 3441 (1993).

[70] Y. H. Ogata, K. Kobayashi, and M. Motoyama, Curr. Opin. Solid St. M. **10**, 163 (2006).

[71] S. Chan, S. Kwon, T.-W. Koo, L. P. Lee, and A. A. Berlin, Adv. Mater. **15**, 1595 (2003).

[72] H. Lin, J. Mock, D. Smith, T. Gao, and M. J. Sailor, J. Phys. Chem. B **108**, 11654 (2004).

[73] R. Miyagawa, K. Fukami, T. Sakka, and Y. H. Ogata, Phys. Status Solidi A **208**, 1471 (2011).

[74] S. Polisski, B. Goller, A. Lapkin, S. Fairclough, and D. Kovalev, Phys. Status Solidi RRL **2**, 132 (2008).

[75] S. Polisski, B. Goller, K. Wilson, D. Kovalev, V. Zaikowskii, and A. Lapkin, J. Catal. **271**, 59 (2010).

[76] R. C. Anderson, R. S. Muller, and C. W. Tobias, Sensor. Actuat. A **21-23**, 835 (1990).

[77] I. Schechter, I. Ben-Chorin, and A. Kux, Anal. Chem. **67**, 3727 (1995).

[78] K. Watanabe, T. Okada, I. Choe, and Y. Sato, Sensor. Actuat. B **33**, 194 (1996).

[79] R. B. Bjorklund, S. Zangooie, and H. Arwin, Appl. Phys. Lett. **69**, 3001 (1996).

[80] P. Snow, E. K. Squire, P. S. J. Russell, and L. Canham, J. Appl. Phys. **86**, 1781 (1999).

[81] L. De Stefano, L. Moretti, A. Lamberti, O. Longo, M. Rocchia, A. M. Rossi, P. Arcari, and I. Rendina, IEEE T. Nanotechnol. **3**, 49 (2004).

[82] M. T. Kelly and A. B. Bocarsly, Coordin. Chem. Rev. **171**, 251 (1998).

[83] M. J. Sailor and E. C. Wu, Adv. Funct. Mater. **19**, 3195 (2009).

[84] G. Barillaro, P. Bruschi, F. Pieri, and L. M. Strambini, Phys. Status Solidi A **204**, 1423 (2007).

[85] G. Barillaro and L. M. Strambini, Sensor. Actuat. B **134**, 585 (2008).

[86] G. Barillaro, P. Bruschi, G. M. Lazzerini, and L. M. Strambini, IEEE Sens. J. **10**, 893 (2010).

[87] K.-P. S. Dancil, D. P. Greiner, and M. J. Sailor, J. Am. Chem. Soc. **121**, 7925 (1999).

[88] A. M. Tinsley-Brown, L. T. Canham, M. Hollings, M. H. Anderson, C. L. Reeves, T. I. Cox, S. Nicklin, D. J. Squirrell, E. Perkins, A. Hutchinson, et al., Phys. Status Solidi A **182**, 547 (2000).

[89] S. Chan, P. M. Fauchet, Y. Li, L. J. Rothberg, and B. L. Miller, Phys. Status Solidi A **182**, 541 (2000).

[90] S. Chan, Y. Li, L. J. Rothberg, B. L. Miller, and P. M. Fauchet, Mat. Sci. Eng. C - Mater. **15**, 277 (2001).

[91] G. Rong, A. Najmaie, J. E. Sipe, and S. M. Weiss, Biosens. Bioelectron. **23**, 1572 (2008).

[92] X. Wei and S. M. Weiss, Opt. Express **19**, 11330 (2011).

[93] S. Chan, S. R. Horner, P. M. Fauchet, and B. L. Miller, J. Am. Chem. Soc. **123**, 11797 (2001).

[94] F. P. Mathew and E. C. Alocilja, Biosens. Bioelectron. **20**, 1656 (2005).

[95] L. M. Bonanno and L. A. DeLouise, Anal. Chem. **82**, 714 (2010).

[96] J. L. Coffer, *Properties of Porous Silicon* (INSPEC, London, United Kingdom, 1997), chap. Porous silicon formation by stain etching, pp. 23–29.

[97] K. W. Kolasinski, Curr. Opin. Solid St. M. **9**, 73 (2005).

[98] N. Noguchi and I. Suemune, Appl. Phys. Lett. **62**, 1429 (1993).

[99] N. Noguchi and I. Suemune, J. Appl. Phys. **75**, 4765 (1994).

[100] X. Li and P. W. Bohn, Appl. Phys. Lett. **77**, 2572 (2000).

[101] K. Peng, Y. Wu, H. Fang, X. Zhong, Y. Xu, and J. Zhu, Angew. Chem. Int. Edit. **44**, 2737 (2005).

[102] M.-L. Zhang, K.-Q. Peng, X. Fan, J.-S. Jie, R.-Q. Zhang, S.-T. Lee, and N.-B. Wong, J. Phys. Chem. C **112**, 4444 (2008).

[103] M. L. Chourou, K. Fukami, T. Sakka, S. Virtanen, and Y. H. Ogata, Electrochim. Acta **55**, 903 (2010).

[104] A. Halimaoui, *Properties of Porous Silicon* (INSPEC, London, United Kingdom, 1997), chap. Porous silicon formation by anodisation, pp. 12–22.

[105] V. Lehmann, *Electrochemistry of Silicon* (Wiley-VCH Verlag GmbH, Weinheim, Germany, 2002).

[106] M. J. Sailor, *Porous Silicon in Practice* (Wiley-VCH Verlag & Co. KGaA, Weinheim, Germany, 2012).

[107] A. Halimaoui, Appl. Phys. Lett. **63**, 1264 (1993).

[108] X. G. Zhang, S. D. Collins, and R. L. Smith, J. Electrochem. Soc. **136**, 1561 (1989).

[109] X. G. Zhang, J. Electrochem. Soc. **151**, C69 (2004).

[110] R. L. Smith and S. D. Collins, J. Appl. Phys. **71**, R1 (1992).

[111] H. Ubara, T. Imura, and A. Hiraki, Solid State Commun. **50**, 673 (1984).

[112] E. Yablonovitch, D. L. Allara, C. Chang, T. Gmitter, and T. B. Bright, Phys. Rev. Lett. **57**, 249 (1986).

[113] V. A. Burrows, Y. J. Chabal, G. S. Higashi, K. Raghavachari, and S. B. Christman, Appl. Phys. Lett. **53**, 998 (1988).

[114] J.-N. Chazalviel and F. Ozanam, J. Appl. Phys. **81**, 7684 (1997).

[115] G. W. Trucks, K. Raghavachari, G. S. Higashi, and Y. J. Chabal, Phys. Rev. Lett. **65**, 504 (1990).

[116] X. G. Zhang, *Electrochemistry of Silicon and Its Oxide* (Kluwer Academic/Plenum Publishers, New York, USA, 2001).

[117] V. Lehmann and U. Gösele, Adv. Mater. **2**, 114 (1992).

[118] H. Gerischer, P. Allongue, and V. Costa-Kieling, Ber. Bunsenges. Phys. Chem. **97**, 753 (1993).

[119] P. Allongue, V. Kieling, and H. Gerischer, Electrochim. Acta **40**, 1353 (1995).

[120] P. Allongue, *Properties of Porous Silicon* (INSPEC, London, United Kingdom, 1997), chap. Porous silicon formation mechanisms, pp. 3–11.

[121] X. G. Zhang, J. Electrochem. Soc. **138**, 3750 (1991).

[122] V. Lehmann, J. Electrochem. Soc. **140**, 2836 (1993).

[123] H. Föll, Appl. Phys. A - Mater. **53**, 8 (1991).

[124] Y. Kang and J. Jorné, Electrochim. Acta **43**, 2389 (1998).

[125] R. Dreiner, J. Electrochem. Soc. **113**, 1210 (1966).

[126] A. Belaidi, M. Safi, F. Ozanam, J.-N. Chazalviel, and O. Gorochov, J. Electrochem. Soc. **146**, 2659 (1999).

[127] V. P. Parkhutik, L. K. Glinenko, and V. A. Labunov, Surf. Technol. **20**, 265 (1983).

[128] V. Parkhutik, Solid State Electron. **43**, 1121 (1999).

[129] P. J. Reece, G. Lérondel, W. H. Zheng, and M. Gal, Appl. Phys. Lett. **81**, 4895 (2002).

[130] L. T. Canham, *Properties of Porous Silicon* (INSPEC, London, United Kingdom, 1997), chap. Pore type, shape, size, volume and surface area in porous silicon, pp. 83–88.

[131] G. Bomchil, R. Herino, K. Barla, and J. C. Pfister, J. Electrochem. Soc. **130**, 1611 (1983).

[132] R. Herino, G. Bomchil, K. Barla, C. Bertrand, and J. L. Ginoux, J. Electrochem. Soc. **134**, 1994 (1987).

[133] R. Hérino, *Properties of Porous Silicon* (INSPEC, London, United Kingdom, 1997), chap. Pore size distribution in porous silicon, pp. 89–96.

[134] M. I. J. Beale, N. G. Chew, M. J. Uren, C. A. G, and J. D. Benjamin, Appl. Phys. Lett. **46**, 86 (1985).

[135] M. I. J. Beale, J. D. Benjamin, M. J. Uren, N. G. Chew, and C. A. G, J. Cryst. Growth **73**, 622 (1985).

[136] S.-F. Chuang, S. D. Collins, and R. L. Smith, Appl. Phys. Lett. **55**, 1540 (1989).

[137] P. Goudeau, A. Naudon, G. Bomchil, and R. Herino, J. Appl. Phys. **66**, 625 (1989).

[138] J. Salonen, M. Björkqvist, and E. Laine, J. Appl. Cryst. **33**, 504 (2000).

[139] E. K. Propst and P. A. Kohl, J. Electrochem. Soc. **141**, 1006 (1994).

[140] E. A. Ponomarev and C. Lévy-Clément, J. Porous Mat. **7**, 51 (2000).

[141] C. Lévy-Clément, A. Lagoubi, and M. Tomkiewicz, J. Electrochem. Soc. **141**, 958 (1994).

[142] T. Osaka, K. Ogasawara, and S. Nakahara, J. Electrochem. Soc. **144**, 3226 (1997).

[143] H. Okayama, K. Fukami, R. Plugaru, T. Sakka, and Y. H. Ogata, J. Electrochem. Soc. **157**, D54 (2010).

[144] J. J. Yon, K. Barla, R. Herino, and G. Bomchil, J. Appl. Phys. **62**, 1042 (1987).

[145] S. Brunauer, P. H. Emmett, and E. Teller, J. Am. Chem. Soc. **60**, 309 (1938).

[146] V. Labunov, V. Bondarenko, L. Glinenko, A. Dorofeev, and L. Tabulina, Thin Solid Films **137**, 123 (1986).

[147] M. Ruike, M. Houzouji, A. Motohashi, N. Murase, A. Kinoshita, and K. Kaneko, Langmuir **12**, 4828 (1996).

[148] H. Sugiyama and O. Nittono, J. Cryst. Growth **103**, 156 (1990).

[149] V. Lehmann and H. Föll, J. Electrochem. Soc. **137**, 653 (1990).

[150] J. Harsányi and H.-U. Habermeier, Microelectron. Eng. **6**, 575 (1987).

[151] S.-F. Chuang, S. D. Collins, and R. L. Smith, Appl. Phys. Lett. **55**, 675 (1989).

[152] C. Jäger, B. Finkenberger, W. Jäger, M. Christophersen, J. Carstensen, and H. Föll, Mater. Sci. Eng. B - Adv. **B69-70**, 199 (2000).

[153] S. Rönnebeck, J. Carstensen, S. Ottow, and H. Föll, Electrochem. Solid St. **2**, 126 (1999).

[154] S. Rönnebeck, S. Ottow, J. Carstensen, and H. Föll, J. Porous Mat. **7**, 353 (2000).

[155] M. Christophersen, J. Carstensen, and H. Föll, Phys. Status Solidi A **182**, 103 (2000).

[156] M. Christophersen, J. Carstensen, and H. Föll, Phys. Status Solidi A **182**, 601 (2000).

[157] R. L. Smith, S.-F. Chuang, and S. D. Collins, J. Electron. Mater. **17**, 533 (1988).

[158] R. L. Smith and S. D. Collins, Phys. Rev. A **39**, 5409 (1989).

[159] S. Frohnhoff, M. Marso, M. G. Berger, M. Thönissen, H. Lüth, and H. Münder, J. Electrochem. Soc. **142**, 615 (1995).

[160] J. Carstensen, R. Prange, G. S. Popkirov, and H. Föll, Appl. Phys. A - Mater. **67**, 459 (1998).

[161] J. Carstensen, M. Christophersen, and H. Föll, Mater. Sci. Eng. B - Adv. **69-70**, 23 (2000).

[162] J. Carstensen, M. Christophersen, G. Hasse, and H. Föll, Phys. Status Solidi A **182**, 63 (2000).

[163] H. Föll, J. Carstensen, M. Christophersen, and G. Hasse, Phys. Status Solidi A **182**, 7 (2000).

[164] G. Hasse, M. Christophersen, J. Carstensen, and H. Föll, Phys. Status Solidi A **182**, 23 (2000).

[165] P. Gupta, V. L. Colvin, and S. M. George, Phys. Rev. B **37**, 8234 (1988).

[166] Y. Kato, T. Ito, and A. Hiraki, Jpn. J. Appl. Phys. **27**, L1406 (1988).

[167] Y. Ogata, H. Niki, T. Sakka, and M. Iwasaki, J. Electrochem. Soc. **142**, 195 (1995).

[168] A. V. Rao, F. Ozanam, and J.-N. Chazalviel, J. Electrochem. Soc. **138**, 153 (1991).

[169] K. H. Bekcmann, Surf. Sci. **3**, 314 (1965).

[170] L. T. Canham, M. R. Houlton, W. Y. Leong, C. Pickering, and J. M. Keen, J. Appl. Phys. **70**, 422 (1991).

[171] W. Theiss, M. Arntzen, S. Hilbrich, M. Wernke, R. Arens-Fischer, and M. G. Berger, Phys. Status Solidi B **190**, 15 (1995).

[172] D. Gräf, M. Grundner, R. Schultz, and L. Mühlhoff, J. Appl. Phys. **68**, 5155 (1990).

[173] P. Gupta, A. C. Dillon, A. S. Bracker, and S. M. George, Surf. Sci. **245**, 360 (1991).

[174] R. C. Anderson, R. S. Muller, and C. W. Tobias, J. Electrochem. Soc. **140**, 1393 (1993).

[175] Y. Ogata, H. Niki, T. Sakka, and M. Iwasaki, J. Electrochem. Soc. **142**, 1595 (1995).

[176] Y. H. Ogata, T. Tsuboi, T. Sakka, and S. Naito, J. Porous Mat. **7**, 63 (2000).

[177] H. Münder, M. G. Berger, S. Frohnhoff, M. Thönissen, H. Lüth, M. Jeske, and J. W. Schultze, J. Lumin. **57**, 223 (1993).

[178] J. Salonen, V.-P. Lehto, and E. Laine, Appl. Surf. Sci. **120**, 191 (1997).

[179] F. Kozlowski, A. Wiedenhofer, W. Wagenseil, P. Steiner, and W. Lang, Thin Solid Films **276**, 284 (1996).

[180] A. Loni, A. J. Simons, P. D. J. Calcott, J. P. Newey, T. I. Cox, and L. T. Canham, Appl. Phys. Lett. **71**, 107 (1997).

[181] H. Koyama, L. Tsybeskov, and P. M. Fauchet, J. Lumin. **80**, 99 (1999).

[182] V. Petrova-Koch, T. Muschik, A. Kux, B. K. Meyer, F. Koch, and V. Lehmann, Appl. Phys. Lett. **61**, 943 (1992).

[183] J. Salonen, V.-P. Lehto, and E. Laine, Appl. Phys. Lett. **70**, 637 (1997).

[184] A. E. Pap, K. Kordás, T. F. George, and S. Leppävuori, J. Phys. Chem. B **108**, 12744 (2004).

[185] J. Salonen, V.-P. Lehto, and E. Laine, J. Porous Mat. **7**, 335 (2000).

[186] A. E. Pap, K. Kordás, G. Tóth, J. Levoska, A. Uusimäki, J. Vähäkangas, S. Leppävuori, and T. F. George, Appl. Phys. Lett. **86**, 041501 (2005).

[187] M. Krüger, S. Hilbrich, M. Thönissen, D. Scheyen, W. Theiß, and H. Lüth, Opt. Commun. **146**, 309 (1998).

[188] J. Riikonen, M. Salomäki, J. van Wonderen, M. Kemell, W. Xu, O. Korhonen, M. Ritala, F. MacMillan, J. Salonen, and V.-P. Lehto, Langmuir **28**, 10573 (2012).

[189] G. Korotcenkov and B. K. Cho, Crit. Rev. Solid State **35**, 153 (2010).

[190] A. Bsiesy, F. Gaspard, R. Herino, M. Ligeon, F. Muller, and J. C. Oberlin, J. Electrochem. Soc. **138**, 3450 (1991).

[191] J. L. Cantin, M. Schoisswohl, A. Grossman, S. Lebib, C. Ortega, H. J. von Bardeleben, . Vázsonyi, G. Jalsovszky, and J. Erostyák, Thin Solid Films **276**, 76 (1996).

[192] M. S. Salem, M. J. Sailor, F. A. Harraz, T. Sakka, and Y. H. Ogata, J. Appl. Phys. **100**, 083520 (2006).

[193] J. H. Song and M. J. Sailor, Inorg. Chem. **37**, 3355 (1998).

[194] G. Mattei, V. Valentini, and V. A. Yakovlev, Surf. Sci. **502-503**, 58 (2002).

[195] U. Frotscher, U. Rossow, M. Ebert, C. Pietryga, W. Richter, M. G. Berger, R. Arens-Fischer, and H. Münder, Thin Solid Films **276**, 36 (1996).

[196] B. Gelloz, A. Kojima, and N. Koshida, Appl. Phys. Lett. **87**, 031107 (2005).

[197] M. Ghulinyan, B. Gelloz, T. Ohta, L. Pavesi, D. J. Lockwood, and N. Koshida, Appl. Phys. Lett. **93**, 061113 (2008).

[198] B. Gelloz and N. Koshida, Thin Solid Films **518**, 3276 (2010).

[199] M. R. Linford and C. E. D. Chidsey, J. Am. Chem. Soc. **115**, 12631 (1993).

[200] M. R. Linford, P. Fenter, P. M. Eisenberger, and C. E. D. Chidsey, J. Am. Chem. Soc. **117**, 3145 (1995).

[201] J. H. Song and M. J. Sailor, J. Am. Chem. Soc. **120**, 2376 (1998).

[202] N. Y. Kim and P. E. Laibinis, J. Am. Chem. Soc. **120**, 4516 (1998).

[203] J. H. Song and M. J. Sailor, Comment. Inorg. Chem. **21**, 69 (1999).

[204] J. M. Buriak, Adv. Mater. **11**, 265 (1999).

[205] M. P. Stewart and J. M. Buriak, Adv. Mater. **12**, 859 (2000).

[206] J. M. Buriak and M. J. Allen, J. Am. Chem. Soc. **120**, 1339 (1998).

[207] J. M. Buriak, M. P. Stewart, T. W. Geders, M. J. Allen, H. C. Choi, J. Smith, D. Raftery, and L. T. Canham, J. Am. Chem. Soc. **121**, 11491 (1999).

[208] M. P. Stewart and J. M. Buriak, Angew. Chem. Int. Edit. **37**, 3257 (1998).

[209] M. P. Stewart and J. M. Buriak, J. Am. Chem. Soc. **123**, 7821 (2001).

[210] J. E. Bateman, R. D. Eagling, D. R. Worrall, B. R. Horrocks, and A. Houlton, Angew. Chem. Int. Edit. **37**, 2683 (1998).

[211] R. Boukherroub, S. Morin, D. D. M. Wayner, and D. J. Lockwood, Phys. Status Solidi A **182**, 117 (2000).

[212] R. Boukherroub, S. Morin, D. D. M. Wayner, F. Bensebaa, G. I. Sproule, J.-M. Baribeau, and D. J. Lockwood, Chem. Mater. **13**, 2002 (2001).

[213] R. Boukherroub, J. T. Wojtyk, D. D. M. Wayner, and D. J. Lockwood, J. Electrochem. Soc. **149**, H59 (2002).

[214] R. Boukherroub, A. Petit, A. Loupy, J.-N. Chazalviel, and F. Ozanam, J. Phys. Chem. B **107**, 13459 (2003).

[215] J. M. Buriak, Chem. Rev. **102**, 1272 (2002).

[216] I. N. Lees, H. Lin, C. A. Canaria, C. Gurtner, M. J. Sailor, and G. M. Miskelly, Langmuir **19**, 9812 (2003).

[217] Y. W. Chung, W. Siekhaus, and G. A. Somorjai, Surf. Sci. **58**, 341 (1976).

[218] J. Yoshinobu, H. Tsuda, M. Onchi, and M. Nishijima, Chem. Phys. Lett. **130**, 170 (1986).

[219] M. Nishijima, J. Yoshinobu, H. Tsuda, and M. Onchi, Surf. Sci. **192**, 383 (1987).

[220] C. C. Cheng, P. A. Taylor, R. M. Wallace, H. Gutleben, L. Clemen, M. L. Colaianni, P. J. Chen, W. H. Weinberg, W. J. Choyke, and J. T. Yates Jr., Thin Solid Films **225**, 196 (1993).

[221] G. Dufour, F. Rochet, F. C. Stedile, C. Poncey, M. De Crescenzi, R. Gunnella, and M. Froment, Phys. Rev. B **56**, 4266 (1997).

[222] J. Salonen, V.-P. Lehto, M. Björkqvist, E. Laine, and L. Niinistö, Phys. Status Solidi A **182**, 123 (2000).

[223] J. Salonen, E. Laine, and L. Niinistö, J. Appl. Phys. **91**, 456 (2002).

[224] J. Salonen, M. Björkqvist, E. Laine, and L. Niinistö, Appl. Surf. Sci. **225**, 389 (2004).

[225] J. Tuura, M. Björkqvist, J. Salonen, and V.-P. Lehto, Mater. Res. Soc. Symp. Proc. **876E**, R8.8.1 (2005).

[226] M. Sarparanta, E. Mäkilä, T. Heikkilä, J. Salonen, E. Kukk, V.-P. Lehto, H. A. Santos, J. Hirvonen, and A. J. Airaksinen, Mol. Pharmaceut. **8**, 1799 (2011).

[227] M. Björkqvist, J. Salonen, and E. Laine, Appl. Surf. Sci. **222**, 269 (2004).

[228] J. Paski, M. Björkqvist, J. Salonen, and V.-P. Lehto, Phys. Status Solidi C **2**, 3379 (2005).

[229] J. Salonen, M. Björkqvist, and J. Paski, Sensor. Actuat. A **116**, 438 (2004).

[230] M. Björkqvist, J. Salonen, J. Paski, and E. Laine, Sensor. Actuat. A **112**, 224 (2004).

[231] J. Salonen, J. Tuura, M. Björkqvist, and V.-P. Lehto, Sensor. Actuat. B **114**, 423 (2006).

[232] J. Tuura, M. Björkqvist, J. Salonen, and V.-P. Lehto, Sensor. Actuat. B **131**, 627 (2008).

[233] M. Björkqvist, J. Salonen, E. Laine, and L. Niinistö, Phys. Status Solidi A **197**, 374 (2003).

[234] B. Sciacca, S. D. Alvarez, F. Geobaldo, and M. J. Sailor, Dalton T. **39**, 10847 (2010).

[235] M. Kovalainen, J. Mönkäre, E. Mäkilä, J. Salonen, V.-P. Lehto, K.-H. Herzig, and K. Järvinen, Pharm. Res. **29**, 837 (2012).

[236] H. A. MacLeod, *Thin Film Optical Filters (Second Edition)* (Adam Hilger Ltd., Bristol, 1986).

[237] M. Born and E. Wolf, *Principles of Optics (Fourth Edition)* (Pergamon Press, Oxford, 1970).

[238] J. D. Jackson, *Classical Electrodynamics (Second Edition)* (John Wiley & Sons, Inc., New York, 1975).

[239] W. J. Duffin, *Electricity and Magnetism (Fourth Edition)* (McGraw-Hill Book Company, London, 1990).

[240] I. Sagnes, A. Halimaoui, G. Vincent, and P. A. Badoz, Appl. Phys. Lett. **62**, 1155 (1993).

[241] J. von Behren, T. van Buuren, M. Zacharias, E. H. Chimowitz, and P. M. Fauchet, Solid State Commun. **105**, 317 (1998).

[242] W. Theiss, Surf. Sci. Rep. **29**, 91 (1997).

[243] W. Theiss, Thin Solid Films **276**, 7 (1996).

[244] J. C. Maxwell-Garnett, Philos. Trans. R. Soc. London, Ser. A **203**, 385 (1904).

[245] D. A. G. Bruggeman, Ann. Phys. **24**, 636 (1935).

[246] H. Looyenga, Physica **31**, 401 (1965).

[247] D. J. Bergman, Phys. Rep. C **43**, 377 (1978).

[248] D. E. Aspnes, J. B. Theeten, and F. Hottier, Phys. Rev. B **20**, 3292 (1979).

[249] M. S. Salem, M. J. Sailor, K. Fukami, T. Sakka, and Y. H. Ogata, J. Appl. Phys. **103**, 083516 (2008).

[250] H. Münder, C. Andrzejak, M. G. Berger, T. Eickhoff, H. Lüth, W. Theiss, U. Rossow, W. Richter, R. Herino, and M. Ligeon, Appl. Surf. Sci. **56-58**, 6 (1992).

[251] F. Ferrieu, A. Halimaoui, and D. Bensahel, Solid State Commun. **84**, 293 (1992).

[252] V. Torres-Costa, R. J. Martín-Palma, and J. M. Martínez-Duart, J. Appl. Phys. **96**, 4197 (2004).

[253] N. Ishikura, M. Fujii, K. Nishida, S. Hayashi, and J. Diener, Opt. Express **16**, 15531 (2008).

[254] Y. Kanemitsu, H. Uto, Y. Masumoto, T. Matsumoto, T. Futagi, and H. Mimura, Phys. Rev. B **48**, 2827 (1993).

[255] J. Salonen, K. Saarinen, J. Peura, J. Viinikanoja, I. Salomaa, E. Laine, and J. Kauppinen, Mater. Res. Soc. Symp. Proc. **486**, 323 (1998).

[256] J. C. Manifacier, J. Gasiot, and J. P. Fillard, J. Phys. E: Sci. Instrum. **9**, 1002 (1976).

[257] K. Kordás, A. E. Pap, S. Beke, and S. Leppävuori, Opt. Mater. **25**, 251 (2004).

[258] A. E. Pap, K. Kordás, J. Vähäkangas, A. Uusimäki, S. Leppävuori, L. Pilon, and S. Szatmári, Opt. Mater. **28**, 506 (2006).

[259] S. M. Weiss and P. M. Fauchet, Phys. Status Solidi A **197**, 556 (2003).

[260] L. De Stefano, L. Moretti, I. Rendina, and A. M. Rossi, Sensor. Actuat. A **104**, 179 (2003).

[261] M. Ghulinyan, C. J. Oton, G. Bonetti, Z. Gaburro, and L. Pavesi, J. Appl. Phys. **93**, 9724 (2003).

[262] L. Dal Negro, C. J. Oton, Z. Gaburro, L. Pavesi, P. Johnson, A. Lagendijk, R. Righini, M. Colocci, and D. S. Wiersma, Phys. Rev. Lett. **90**, 055501 (2003).

[263] V. Agarval, J. A. Soto-Urueta, D. Becerra, and M. E. Mora-Ramos, Photonic. Nanostruct. **3**, 155 (2005).

[264] L. Moretti, I. Rea, L. Rotiroti, I. Rendina, G. Abbate, A. Marino, and L. De Stefano, Opt. Express **14**, 6264 (2006).

[265] L. Moretti, I. Rea, L. De Stefano, and I. Rendina, Appl. Phys. Lett. **90**, 191112 (2007).

[266] B. G. Bovard, Appl. Optics **32**, 5427 (1993).

[267] J. A. Dobrowolski, *Handbook of Optics, Volume I (Second Edition)* (McGraw-Hill, Inc., 1995), chap. 42, pp. 42.1–42.130.

[268] N. Perelman and I. Averbukh, J. Appl. Phys. **79**, 2839 (1996).

[269] E. Lorenzo, C. J. Oton, N. E. Capuj, M. Ghulinyan, D. Navarro-Urrios, Z. Gaburro, and L. Pavesi, Appl. Optics **44**, 5415 (2005).

[270] M. S. Salem, M. J. Sailor, T. Sakka, and Y. H. Ogata, J. Appl. Phys. **101**, 063503 (2007).

[271] S. O. Meade, M. S. Yoon, K. H. Ahn, and M. J. Sailor, Adv. Mater. **16**, 1811 (2004).

[272] W. H. Southwell, Appl. Optics **28**, 5091 (1989).

[273] H. A. Abu-Safia, A. I. Al-Sharif, and I. O. Abu Aljarayesh, Appl. Optics **32**, 4831 (1993).

[274] W. H. Southwell and R. L. Hall, Appl. Optics **28**, 2949 (1989).

[275] S. Ilyas, T. Böcking, K. Kilian, P. J. Reece, J. Gooding, K. Gaus, and M. Gal, Opt. Mater. **29**, 619 (2007).

[276] S. M. Weiss, G. Rong, and J. L. Lawrie, Physica E **41**, 1071 (2009).

[277] S. Ozdemir and J. L. Gole, Curr. Opin. Solid St. M. **11**, 92 (2007).

[278] P. A. Webb and C. Orr, *Analytical Methods in Fine Particle Technology* (Micromeritics Instrument Corp, 1997).

[279] A. Iraji Zad, F. Rahimi, M. Chavoshi, and M. M. Ahadian, Sensor. Actuat. B **100**, 341 (2004).

[280] M. Archer, M. Christophersen, and P. M. Fauchet, Sensor. Actuat. B **106**, 347 (2005).

[281] C. J. Oton, L. Pancheri, Z. Gaburro, L. Pavesi, C. Baratto, G. Faglia, and G. Sberveglieri, Phys. Status Solidi A **197**, 523 (2003).

[282] G. Barillaro, A. Nannini, and F. Pieri, Sensor. Actuat. B **93**, 263 (2003).

[283] G. Barillaro, A. Diligenti, A. Nannini, L. M. Strambini, E. Comini, and G. Sberveglieri, IEEE Sens. J. **6**, 19 (2006).

[284] M. Björkqvist, J. Paski, J. Salonen, and V.-P. Lehto, IEEE Sens. J. **6**, 542 (2006).

[285] J. M. Lauerhaas, C. M. Credo, J. L. Heinrich, and M. J. Sailor, J. Am. Chem. Soc. **114**, 1911 (1992).

[286] J. M. Lauerhaas and M. J. Sailor, Science **261**, 1567 (1993).

[287] S. Zangooie, R. Bjorklund, and H. Arwin, Sensor. Actuat. B **43**, 168 (1997).

[288] V. Mulloni and L. Pavesi, Appl. Phys. Lett. **76**, 2523 (2000).

[289] L. De Stefano, L. Moretti, I. Rendina, and A. M. Rossi, Sensor. Actuat. B **100**, 168 (2004).

[290] H. F. Arrand, T. M. Benson, A. Loni, R. Arens-Fischer, M. Krüger, M. Thönissen, H. Lüth, and S. Kershaw, IEEE Photonic. Tech. L. **10**, 1467 (1998).

[291] B. H. King, A. M. Ruminski, J. L. Snyder, and M. J. Sailor, Adv. Mater. **19**, 4530 (2007).

[292] A. M. Ruminski, B. H. King, J. Salonen, J. L. Snyder, and M. J. Sailor, Adv. Funct. Mater. **20**, 2874 (2010).

[293] J. R. Link and M. J. Sailor, P. Natl. Acad. Sci. USA **100**, 10607 (2003).

[294] A. M. Ruminski, M. M. Moore, and M. J. Sailor, Adv. Funct. Mater. **18**, 3418 (2008).

[295] A. M. Ruminski, G. Barillaro, C. Chaffin, and M. J. Sailor, Adv. Funct. Mater. **21**, 1511 (2011).

[296] S. E. Létant and M. J. Sailor, Adv. Mater. **12**, 355 (2000).

[297] S. E. Létant, S. Content, T. T. Tan, F. Zenhausern, and M. J. Sailor, Sensor. Actuat. B **69**, 193 (2000).

[298] V. Mulloni, Z. Gaburro, and L. Pavesi, Phys. Status Solidi A **182**, 479 (2000).

[299] C. Baratto, G. Faglia, G. Sberveglieri, Z. Gaburro, L. Pancheri, C. Oton, and L. Pavesi, Sensors **2**, 121 (2002).

[300] T. Hutter and S. Ruschin, IEEE Sens. J. **10**, 97 (2010).

[301] S.-H. Park, D. Seo, Y.-Y. Kim, and K.-W. Lee, Sensor. Actuat. B **147**, 775 (2010).

[302] V. Polishchuk, E. Souteyrand, J. R. Martin, V. I. Strikha, and V. A. Skryshevsky, Anal. Chim. Acta **375**, 205 (1998).

[303] C. Tsamis, L. Tsoura, A. G. Nassiopoulou, A. Travlos, C. E. Salmas, K. S. Hatzilyberis, and G. P. Androutsopoulos, IEEE Sens. J. **2**, 89 (2002).

[304] H. Lin, T. Gao, J. Fantini, and M. J. Sailor, Langmuir **20**, 5104 (2004).

[305] J. M. Palmer, *Handbook of Optics, Volume II (Second Edition)* (McGraw-Hill, Inc., 1995), chap. 25, pp. 25.1–25.25.

[306] P. R. Griffiths and J. A. de Haseth, *Fourier Transform Infrared Spectrometry* (John Wiley & Sons Inc., 1986).

[307] F. Rouquerol, J. Rouquerol, and K. Sing, *Adsorption by Powders and Porous Solids* (Academic Press, 1999).

[308] E. P. Barett, L. G. Joyner, and P. P. Halenda, J. Am. Chem. Soc. **73**, 373 (1951).

[309] T. E. Everhart and R. F. M. Thornley, J. Sci. Instrum. **37**, 246 (1960).

[310] J. I. Goldstein, C. E. Lyman, D. E. Newbury, E. Lifshin, P. Echlin, L. Sawyer, D. C. Joy, and J. R. Michael, *Scanning Electron Microscopy and X-Ray Microanalysis, Third Edition* (Kluwer Academic/Plenum Publishers, New York, USA, 2003).

[311] J. F. Watts and J. Wolstenholme, *An Introduction to Surface Analysis by XPS and AES* (John Wiley & Sons Ltd, West Sussex, England, 2003).

[312] D. Briggs and M. P. Seah, eds., *Practical Surface Analysis, Second Edition* (John Wiley & Sons Ltd, West Sussex, England, 1992).

[313] M. Björkqvist, J. Salonen, J. Tuura, T. Jalkanen, and V.-P. Lehto, Phys. Status Solidi C **6**, 1769 (2009).

[314] T. Jalkanen, V. Torres-Costa, E. Mäkilä, T. Sakka, Y. H. Ogata, and J. Salonen (manuscript in preparation).